Table 1
Microstructure indices analysis of fusion mass by three-dimensional microcomputed tomography

	2 wk after surgery		4 wk after surgery		6 wk after surgery	
Parameters	CNT group	TPTD group	CNT group	TPTD group	CNT group	TPTD group
BV (mm^3)	1.4±0.8	2.1±0.9	3.2±1.0	6.1±1.3**	3.5±1.2	5.5±2.1*
BV/TV (%)	45.0±15.8	50.3±8.6	58.4±10.1	71.7±9.0**	60.1±11.3	63.9±11.3
Tb.N (1/mm)	4.5±2.8	4.2±1.0	4.9±1.2	4.8±0.4	4.7±0.7	4.3±0.5
Tb.Th (μm)	108.7±16.5	118.3±16.0	124.6±11.4	151.2±17.0**	129.0±13.8	152.3±21.0*
Tb.Sp (μm)	283.6±177.1	172.6±37.5	105.5±46.1	71.6±42.3	93.2±36.1	99.7±51.9

BV, bone volume; TV, tissue volume; CNT, control; Tb.N, trabecular number; Tb.Th, trabecular thickness; Tb.Sp, trabecular separation; TPTD, teriparatide.
*p<.05 versus CNT group.
**p<.01 versus CNT group.

Bone microstructural parameters of adjacent vertebrae (L6) assessed by microcomputed tomography

At the L6 vertebrae adjacent to the surgical site, BV/TV continuously increased in both groups, and there were significant differences between the groups at 4 and 6 weeks after surgery. Similarly, there were significant differences in trabecular and cortical BMDs between the groups at 4 and 6 weeks after surgery (Table 2).

Fusion assessment

Fusion rate was higher in the TPTD group than in the CNT group (CNT, 5/9 [56%]; TPTD, 8/9 [89%]), although the statistical difference was not obtained (χ^2=2.49, p=.11).

Bone histomorphometry in fusion mass

Table 3 shows the findings for bone histomorphometrical parameters of the fusion mass at 6 weeks after surgery. Mineral apposition rate, N.Ob/BS, and OS/BS were significantly higher in the TPTD group than in the CNT group. In contrast, ES/BS was significantly higher in the CNT group than the TPTD group and N.Oc/BS was higher in the CNT group than the TPTD group. Bone histomorphometry revealed that TPTD accelerated the modeling and remodeling processes predominantly by stimulating bone formation at the fusion mass by 6 weeks after surgery (Fig. 3).

Serum bone metabolism markers

The TRACP-5b levels were significantly higher in the TPTD group than in the CNT group (CNT, 2.1±0.3 U/L; TPTD, 2.8±0.9 U/L; p<.05). However, OC levels were not significantly different between the groups (CNT, 66.1±19.4 ng/mL; TPTD, 55.0±10.6 ng/mL; p=.17).

Discussion

Our study shows that intermittent TPTD administration during continuous GC exposure accelerates the bone modeling and remodeling processes predominantly by stimulating bone formation at the fusion mass, increasing the fusion rate, and improving the bone microarchitecture of vertebrae adjacent to the surgical site in a rat model of spinal fusion.

Bostrom et al. [30] examined the effect of PTH-related peptide treatment on fracture healing in a rabbit model of GIOP, and they found that intermittent administration of the peptide improved the radiographic union rate and the mechanical strength of the fracture site. Other studies also have shown that intermittent administration of TPTD stimulates fracture healing in animal models [31,32]. Although the mechanism by which TPTD and its analog improve bone healing in GC-treated animals is not completely understood, these agents are considered to suppress osteoblast apoptosis and dysfunction [33,34]. Recently, GC-induced suppression in bone formation was described as

Table 2
Microstructure indices analysis of vertebrae adjacent to the surgical site (L6) by three-dimensional microcomputed tomography

	2 wk after surgery		4 wk after surgery		6 wk after surgery	
Parameters	CNT group	TPTD group	CNT group	TPTD group	CNT group	TPTD group
BMD.tr (mg/cm^3)	229.3±24.7	228.0±19.9	246.6±32.7	285.3±28.3*	263.4±37.0	309.2±34.3*
BMD.cr (mg/cm^3)	374.8±32.0	378.8±20.3	411.6±31.8	439.7±21.8*	416.0±31.0	450.1±20.1*
BV/TV (%)	42.2±7.3	41.7±5.7	49.1±5.3	54.9±4.2*	51.6±6.2	57.8±5.9*
Tb.N (1/mm)	1.1±0.1	1.0±0.1	1.1±0.1	1.1±0.2	1.2±0.1	1.1±0.1
Tb.Th (μm)	208.8±10.3	204.9±11.7	213.3±10.4	233.6±16.4**	232.3±8.7	241.1±18.1
Tb.Sp (μm)	233.2±31.3	241.6±18.1	211.8±38.2	215.9±20.8	202.8±16.3	208.8±20.9

BMD.tr, bone mineral density of trabecular bone; BMD.cr, bone mineral density of cortical bone; BV/TV, bone volume/tissue volume; CNT, control; Tb.N, trabecular number; Tb.Th, trabecular thickness; Tb.Sp, trabecular separation; TPTD, teriparatide.
*p<.05 versus CNT group.
**p<.01 versus CNT group.

Table 3
Bone histomorphometrical parameters of fusion mass

Parameters	CNT group	TPTD group
OS/BS (%)	47.0±14.8	67.0±11.3*
ES/BS (%)	35.9±8.2	18.8±6.3**
dLs/BS (%)	24.0±10.4	32.9±13.5
sLs/BS (%)	29.0±4.4	28.2±10.6
N.Ob/BS (N/mm)	23.4±8.8	48.9±9.9**
N.Oc/BS (N/mm)	4.5±0.9	2.9±1.3
MS/BS (%)	38.5±8.9	47.0±10.0
MAR (μm/day)	3.1±0.5	4.6±0.4**
BFR/BS (mm^3/mm^2 per y)	0.4±0.2	0.8±0.2*
BRs.R (mm^3/mm^2 per y)	0.1±0.04	1.5±1.7

BS, bone surface; BFR, bone formation rate, BRs.R, bone resorption rate; CNT, control; dLs, double-labeled surface; ES, eroded surface; MAR, mineral apposition rate; MS, mineralizing surface; N.Ob, osteoblast number; N.Oc, osteoclast number; OS, osteoid surface; sLs, single-labeled surface; TPTD, teriparatide.

*p<.05 versus CNT group.

**p<.01 versus CNT group.

being the result of upregulation of Wnt/β-catenin antagonists, such as Dickkopf-related protein 1. TPTD targets osteocytes and reduces the expression of Wnt/β-catenin antagonists, sclerostin, and Dickkopf-related protein 1 [35]. For patients with GIOP, intermittent TPTD administration is a logical bone anabolic therapy that can cancel the activation of Wnt/β-catenin antagonists by GCs.

Lawrence et al. [27] reported that intermittent administration of TPTD (20 μg/kg per day) in a healthy animal model of spinal fusion led to an increased fusion rate, as detected on the manual palpation test (fusion rate at 6 weeks after surgery: 37% in the CNT group and 52% in the TPTD group), and also increased serum OC levels in a rat model of spinal fusion. Abe et al. [25] reported that intermittent administration of TPTD (40 μg/kg per day) enhanced bone turnover predominantly by increasing bone formation at the graft site and led to the acceleration of spinal fusion in a rat model (fusion rate at 6 weeks after surgery: 86% in the CNT group and 100% in the TPTD group). Ming et al. [36] also reported similar effects in a rat model of spinal fusion, noting that BMD, bone mineral content, and trabecular area of the lumbar vertebrae (which was not the surgical site) were significantly higher in animals that received TPTD (five times a week, one group receive 4 μg/kg and the other received 23 μg/kg) than in those not receiving it, and these effects were dose-dependent. Qiu et al. [37] reported that TPTD (30 μg/kg per day) enhanced the quantity of the fusion callus and reduced the healing time for spinal fusion in ovariectomized female rats with osteoporosis. At 6 weeks after surgery, the TPTD treated group had a significantly higher fusion rate than the CNT group (fusion rate at 6 weeks after surgery: 56% in the CNT group and 89% in the TPTD group).

In our study, the fusion rate during GC exposure was higher in the TPTD group than in the CNT group, although the statistical difference was not obtained. This finding is similar to that of several earlier studies using healthy animals and ovariectomized animals with osteoporosis. Values for the microstructural parameters relevant to trabecular

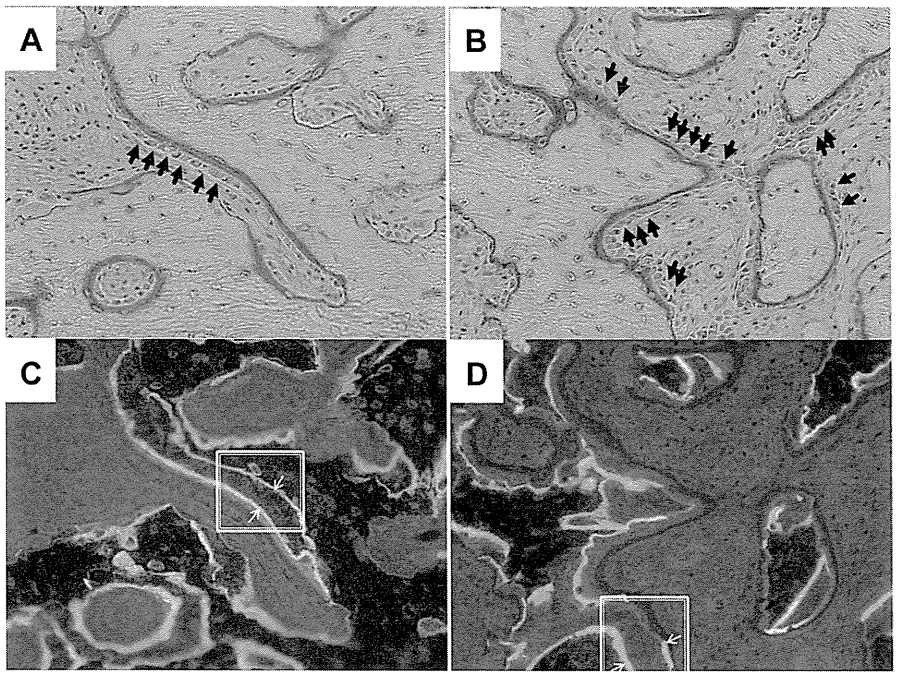

Fig. 3. Histologic features of fusion mass. The upper panels (A and B) show data obtained under natural light, and the lower panels (C and D) show data obtained under fluorescent light. Active osteoblast cells (black arrows) were more frequently observed in the (B) teriparatide (TPTD) group specimens than in the (A) control (CNT) group specimens. The specimens in the (D) TPTD group had a larger calcein-labeled surface area (between the two white arrows) than the (C) CNT group.

bone of the fusion mass increased and reached a peak by 4 weeks after surgery in the TPTD group, and these values were significantly greater than in the CNT group at 4 and 6 weeks after surgery. We found the peak for these parameters to be delayed in comparison with the findings of Abe et al. [25], who reported a peak at 2 weeks after surgery and significantly greater values in their TPTD group than in their CNT group. The impairment of bone formation because of prolonged GC exposure may retard the effect of TPTD in spinal fusion. This retardation may be resolved by accelerating the beginning TPTD administration.

We found that in bone histomorphologic analysis, values for bone formation parameters such as MAR, N.Ob/BS, and OS/BS were significantly higher in the TPTD group than in the CNT group. Our histologic findings suggest that bone turnover was accelerated in the TPTD group by stimulating bone formation predominantly at the fusion mass, as others have found [25]. We found that serum OC levels were not greater in the TPTD group than in the CNT group, unlike the findings in previous studies [25,27]. We collected blood samples at 6 weeks after surgery, and we believe that the peak of bone formation and resorption occurred before that point. In addition, OC is secreted by differentiated mature osteoblasts [38], and there is a possibility that the number of mature osteoblasts decreased in rats with GIOP.

Serum TRACP-5b levels were significantly greater in the TPTD group than in the CNT group in our study, and bone resorption was enhanced systemically in the TPTD group. However, values for bone resorption parameters of the fusion mass such as ES/BS and N.Oc/BS were lower in the TPTD group than in the CNT group, in contrast with the findings of Abe et al. [25]. In our study, fusion rate for the CNT group was 56%, but in the study by Abe et al. [25], the fusion rate for the CNT group was 86% at 4 and 6 weeks after surgery. Local enhancement of bone resorption in our CNT group may account for micromotion in the specimens with nonunion.

Ohtori et al. [39] reported that daily subcutaneous TPTD injection in postmenopausal women with osteoporosis after posterolateral fusion surgery produced better bone union than oral bisphosphonate. They also reported that TPTD treatment reduced the healing time for spinal fusion. However, there have been no studies of the effect of intermittent TPTD administration on the union of grafted bone in spinal fusion surgery of patients with GIOP. DeWald and Stanley [10] reported that spinal stabilization surgery in patients with poor bone stock is associated with a high rate of complications, such as vertebral fracture adjacent to the surgical site. Toyone et al. [11] reported that postmenopausal women who underwent lumbar spine instrumentation surgery were susceptible to developing vertebral fractures within 2 years after surgery. Van Staa et al. [40] reported that patients taking GC had higher fracture risk than those who did not take it, even when the BMD was similar for both groups. All of those findings make it clear that patients with severe osteoporosis such as GIOP are at high risk for subsequent vertebral fracture or instrumentation failure after spinal fusion, and thus an effective therapy is necessary not only for delayed union of the fusion mass but also for bone loss at the vertebrae adjacent to the surgical site. Our bone microstructural analysis showed that BMD and BV/TV at L6 were significantly greater in the TPTD group than in the CNT group at 4 weeks after surgery, similar to the findings of Ming et al. [36], who used a healthy rat model of spinal fusion, and Tseng et al. [41] reported clinical data showing that the intermittent administration of TPTD reduced the risk of the new vertebral compression fractures in the treatment of new-onset adjacent compression fractures after percutaneous vertebroplasty. In view of our findings and those of Ming et al. [36] and Tseng et al. [41], it is apparent that the risk of adjacent vertebral fracture or instrumentation failure after spinal fusion surgery in patients with GIOP can be reduced by the intermittent administration of TPTD.

There are some limitations to our study. First, the mechanical environment and healing process of the fusion mass of humans is thought to be different from that of rats because the latter are four-footed animals. Therefore, our results are not completely applicable to graft bone healing in spinal fusion surgery in humans. Second, there are no spinal fusion controls without MP exposure given placebo normal saline injections, and the degree at which TPTD offset the GC effects was not assessed in this study. Further studies to assess the degree at which TPTD offset the GC effects are thought to be necessary. Third, although we determined the study period based on several previous studies [25,27], the study period was relatively short because 11% of the TPTD group was not fused after TPTD administration for 6 weeks. We think that future studies to explore the duration of TPTD therapy to maximize graft unions are necessary. Furthermore, it is unclear whether the dose of TPTD that we used would be adequate in humans. The clinical dose for osteoporosis in humans is 20 μg/d (which in a 60 kg person translates to 0.33 μg/kg per day). However, we used a dose of approximately 29 μg/kg per day, and studies of other animal models of spinal fusion have reported the use of 4 to 40 μg/kg per day to achieve an anabolic effect for graft bone healing. The effective dose is considered to be different for humans and animals because the response and metabolism of TPTD differs among species. However, it is possible that more than an osteoporosis dose of TPTD may be necessary to enhance graft bone repair after spinal fusion surgery in humans with GIOP. Therefore, clinical trials must be conducted to ascertain the effective dose of TPTD in GIOP.

Conclusions

The intermittent administration of TPTD accelerated the bone modeling and remodeling processes after spinal fusion in a rat model with GIOP by stimulating bone formation predominantly at the fusion mass, increasing the fusion

rate, and improving the bone microarchitecture of the vertebrae adjacent to the surgical site.

Acknowledgments

We thank Akemi Ito of the Ito Bone Histomorphometry Institute for providing bone histomorphometry measurements. We also thank Asahi Kasei for supplying teriparatide. Medical editor Katharine O'Moore-Klopf, ELS (East Setauket, NY, USA) provided professional English-language editing of this article.

References

[1] Lane NE, Lukert B. The science and therapy of glucocorticoid-induced bone loss. Endocrinol Metab Clin North Am 1998;27:465–83.
[2] Bultink IE, Baden M, Lems WF. Glucocorticoid-induced osteoporosis: an update on current pharmacotherapy and future directions. Expert Opin Pharmacother 2013;14:185–97.
[3] O'Brien CA, Jia D, Plotkin LI, Bellido T, Powers CC, Stewart SA, et al. Glucocorticoid act directly on osteoblasts and osteocytes to induce their apoptosis and reduce bone formation and strength. Endocrinology 2004;145:1835–41.
[4] Liu Y, Porta A, Peng X, Gengaro K, Cunningham EB, Li H, et al. Prevention of glucocorticoid-induced apoptosis in osteocytes and osteoblasts by carbindin-D28k. J Bone Miner Res 2004;19:479–90.
[5] Dalle Carbonare L, Arlot ME, Chavassieux PM, Roux JP, Portero NR, Meunier PJ. Comparison of trabecular bone microarchitecture and remodeling in glucocorticoid-induced and postmenopausal osteoporosis. J Bone Miner Res 2001;16:97–103.
[6] Bridwell KH, Sedgewick TA, O'Brien MF, Lenke LG, Baldus C. The role of fusion and instrumentation in the treatment of degenerative spondylolisthesis with spinal stenosis. J Spinal Disord 1993;6:461–72.
[7] McGuire RA, Amundson GM. The use of primary internal fixation in spondylolisthesis. Spine 1993;18:1662–72.
[8] West JL III, Bradford DS, Ogilvie JW. Results of spinal arthrodesis with pedicle screw-plate fixation. J Bone Joint Surg Am 1991;73:1179–84.
[9] Zdeblick TA. A prospective, randomized study of lumbar fusion. Preliminary results. Spine 1993;18:983–91.
[10] DeWald CJ, Stanley T. Instrumentation-related complications of multilevel fusions for adult spinal deformity patients over age 65: surgical considerations and treatment options in patients with poor bone quality. Spine 2006;31(19 Suppl):S144–51.
[11] Toyone T, Ozawa T, Kamikawa K, Watanabe A, Matsuki K, Yamashita T, et al. Subsequent vertebral fractures following spinal fusion surgery for degenerative lumbar disease: a mean ten-year follow-up. Spine 2010;35:1915–8.
[12] Ito M, Kaneda K. Osteopenia: vertebrectomy and fusion. In: Herkowitz H, Dvorak J, Bell G, Nordin M, Grob D, eds. The lumbar spine. 3rd ed. Hagerstown, MD, USA: Lippincott Williams & Wilkins, 2004:683–9.
[13] Dempster DW, Cosman F, Parisien M, Shen V, Lindsay R. Anabolic actions of parathyroid hormone on bone. Endocr Rev 1993;14:690–709.
[14] Dempster DW, Cosman F, Kurland ES, Zhou H, Nieves J, Woelfert L, et al. Effects of daily treatment with parathyroid hormone on bone microarchitecture and turnover in patients with osteoporosis: a paired biopsy study. J Bone Miner Res 2001;16:1846–53.
[15] Finkelstein JS, Klibanski A, Schaefer EH, Hornstein MD, Schiff I, Neer RM. Parathyroid hormone for the prevention of bone loss induced by estrogen deficiency. N Engl J Med 1994;331:1618–23.
[16] Lindsay R, Nieves J, Formica C, Henneman E, Woelfert L, Shen V, et al. Randomised controlled study of effect of parathyroid hormone on vertebral-bone mass and fracture incidence among postmenopausal women on oestrogen with osteoporosis. Lancet 1997;350:550–5.
[17] Neer RM, Arnaud CD, Zanchetta JR, Prince R, Gaich GA, Reginster JY, et al. Effect of parathyroid hormone (1-34) on fractures and bone mineral density in postmenopausal women with osteoporosis. N Engl J Med 2001;344:1434–41.
[18] Saag KG, Zanchetta JR, Devogelaer JP, Adler RA, Eastell R, See K, et al. Effects of teriparatide versus alendronate for treating glucocorticoid-induced osteoporosis: thirty-six-month results of a randomized, double-blind, controlled trial. Arthritis Rheum 2009;60:3346–55.
[19] Saag KG, Shane E, Boonen S, Marin F, Donley DW, Taylor KA, et al. Teriparatide or alendronate in glucocorticoid-induced osteoporosis. N Engl J Med 2007;357:2028–39.
[20] Karras D, Stoykov I, Lems WF, Langdahl BL, Ljunggren Ö, Barrett A, et al. Effectiveness of teriparatide in postmenopausal women with osteoporosis and glucocorticoid use: 3-year results from the EFOS study. J Rheumatol 2012;39:600–9.
[21] D'Amelio P, Tamone C, Sassi F, D'Amico L, Roato I, Patane S, et al. Teriparatide increases the maturation of circulating osteoblast precursors. Osteoporos Int 2012;23:1245–53.
[22] Qin L, Raggatt LJ, Partridge NC. Parathyroid hormone: a double-edged sword for bone metabolism. Trends Endocrinol Metab 2004;15:60–5.
[23] Datta NS. Osteoporotic fracture and parathyroid hormone. World J Orthop 2011;2:67–74.
[24] Hulley PA, Conradie MM, Langeveldt CR, Hough FS. Glucocorticoid-induced osteoporosis in the rat is prevented by the tyrosine phosphatase inhibitor, sodium orthovanadate. Bone 2002;31:220–9.
[25] Abe Y, Takahata M, Ito M, Irie K, Abumi K, Minami A. Enhancement of graft bone healing by intermittent administration of human parathyroid hormone (1-34) in a rat spinal arthrodesis model. Bone 2007;41:775–85.
[26] Kawai S, Takagi Y, Kaneko S, Kurosawa T. Effect of three types of mixed anesthetic agents alternate to ketamine in mice. Exp Anim 2011;60:481–7.
[27] Lawrence JP, Ennis F, White AP, Magit D, Polzhofer G, Drespe I, et al. Effect of daily parathyroid hormone (1-34) on lumbar fusion in a rat model. Spine J 2006;6:385–90.
[28] Grauer JN, Patel TC, Erulkar JS, Troiano NW, Panjabi MM, Friedlaender GE. 2000 Young Investigator Research Award winner. Evaluation of OP-1 as a graft substitute for intertransverse process lumbar fusion. Spine 2001;26:127–33.
[29] Dempster DW, Compston JE, Drezner MK, Glorieux FH, Kanis JA, Malluche H, et al. Standardized nomenclature, symbols, and units for bone histomorphometry: a 2012 update of the report of the ASBMR Histomorphometry Nomenclature Committee. J Bone Miner Res 2013;28:2–17.
[30] Bostrom MP, Gamradt SC, Asnis P, Vickery BH, Hill E, Avnur Z, et al. Parathyroid hormone-related protein analog RS-66271 is an effective therapy for impaired bone healing in rabbits on corticosteroid therapy. Bone 2000;26:437–42.
[31] Nakajima A, Shimoji N, Shiomi K, Shimizu S, Moriya H, Einhorn TA, et al. Mechanisms for the enhancement of fracture healing in rats treated with intermittent low-dose human parathyroid hormone (1-34). J Bone Miner Res 2002;17:2038–47.
[32] Jahng JS, Kim HW. Effect of intermittent administration of parathyroid hormone on fracture healing in ovariectomized rats. Orthopedics 2000;23:1089–94.
[33] Jilka RL, Weinstein RS, Bellido T, Roberson P, Parfitt AM, Manolagas SC. Increased bone formation by prevention of osteoblast apoptosis with parathyroid hormone. J Clin Invest 1999;104:439–46.
[34] Yao W, Cheng Z, Pham A, Busse C, Zimmermann EA, Ritchie RO, et al. Glucocorticoid-induced bone loss in mice can be reversed by the actions of parathyroid hormone and risedronate on different

pathways for bone formation and mineralization. Arthritis Rheum 2008;58:3485–97.

[35] Baron R, Hesse E. Update on bone anabolics in osteoporosis treatment: rationale, current status, and perspectives. J Clin Endocrinol Metab 2012;97:311–25.

[36] Ming N, Cheng JT, Rui YF, Chan KM, Kuhstoss S, Ma YL, et al. Dose-dependent enhancement of spinal fusion in rats with teriparatide (PTH[1-34]). Spine 2012;37:1275–82.

[37] Qiu Z, Wei L, Liu J, Sochacki KR, Liu X, Bishop C, et al. Effect of intermittent PTH (1-34) on posterolateral spinal fusion with iliac crest bone graft in an ovariectomized rat model. Osteoporos Int 2013;24:2693–700.

[38] Neugebauer BM, Moore MA, Broess M, Gerstenfeld LC, Hauschka PV. Characterization of structural sequences in the chicken osteocalcin gene: expression of osteocalcin by maturing osteoblasts and by hypertrophic chondrocytes in vitro. J Bone Miner Res 1995; 10:157–63.

[39] Ohtori S, Inoue G, Orita S, Yamauchi K, Eguchi Y, Ochiai N, et al. Teriparatide accelerates lumbar posterolateral fusion in women with postmenopausal osteoporosis: prospective study. Spine 2012;37: E1464–8.

[40] Van Staa TP, Laan RF, Barton IP, Cohen S, Reid DM, Cooper C. Bone density threshold and other predictors of vertebral fracture in patients receiving oral glucocorticoid therapy. Arthritis Rheum 2003;48:3224–9.

[41] Tseng YY, Su CH, Lui TN, Yeh YS, Yeh SH. Prospective comparison of the therapeutic effect of teriparatide with that of combined vertebroplasty with antiresorptive agents for the treatment of new-onset adjacent vertebral compression fracture after percutaneous vertebroplasty. Osteoporos Int 2012;23:1613–22.

nature COMMUNICATIONS

ARTICLE

Received 11 Feb 2014 | Accepted 6 Mar 2014 | Published 7 Apr 2014

DOI: 10.1038/ncomms4591 OPEN

Ultra-sensitive liquid biopsy of circulating extracellular vesicles using ExoScreen

Yusuke Yoshioka[1,2,3], Nobuyoshi Kosaka[1], Yuki Konishi[1,4], Hideki Ohta[5], Hiroyuki Okamoto[5], Hikaru Sonoda[5], Ryoji Nonaka[6], Hirofumi Yamamoto[6], Hideshi Ishii[7], Masaki Mori[6], Koh Furuta[8], Takeshi Nakajima[9], Hiroshi Hayashi[4], Hajime Sugisaki[4], Hiroko Higashimoto[4], Takashi Kato[2], Fumitaka Takeshita[1] & Takahiro Ochiya[1]

Cancer cells secrete small membranous extracellular vesicles (EVs) into their microenvironment and circulation. Although their potential as cancer biomarkers has been promising, the identification and quantification of EVs in clinical samples remains challenging. Here we describe a sensitive and rapid analytical technique for profiling circulating EVs directly from blood samples of patients with colorectal cancer. EVs are captured by two types of antibodies and are detected by photosensitizer-beads, which enables us to detect cancer-derived EVs without a purification step. We also show that circulating EVs can be used for detection of colorectal cancer using the antigen CD147, which is embedded in cancer-linked EVs. This work describes a new liquid biopsy technique to sensitively detect disease-specific circulating EVs and provides perspectives in translational medicine from the standpoint of diagnosis and therapy.

[1] Division of Molecular and Cellular Medicine, National Cancer Center Research Institute, Chuo-ku, Tokyo 104-0045, Japan. [2] Integrative Bioscience and Biomedical Engineering, Graduate School of Advanced Science and Engineering, Waseda University, Shinjuku, Tokyo 162-8480, Japan. [3] Research Fellow of the Japan Society for the Promotion of Science (JSPS), Chiyoda-Ku, Tokyo 102-0083, Japan. [4] R&D Department, SRL Inc., Hino-shi, Tokyo 191-0002, Japan. [5] Diagnostics Division, Shionogi & Co., LTD., Settsu-shi, Osaka 566-0022, Japan. [6] Department of Gastroenterological Surgery, Graduated School of Medicine, Osaka University, Suita, Osaka 565-0871, Japan. [7] Department of Frontier Science for Cancer and Chemotherapy, Osaka University, Graduate School of Medicine, Suita, Osaka 565-0871, Japan. [8] Division of Clinical Laboratories, National Cancer Center Hospital, Chuo-ku Tokyo, 104-0045, Japan. [9] Endoscopy Division, National Cancer Center Hospital, Chuo-ku, Tokyo 104-0045, Japan. Correspondence and requests for materials should be addressed to T.O. (email: tochiya@ncc.go.jp).

Cancer cells secrete various types of humoral factors into their microenvironment that are biomarkers for disease diagnosis and prognosis, including cytokines, chemokines and nucleic acids. Extracellular vesicles (EVs), including exosome and microvesicles from cancer cells, have also been found in the blood of cancer patients[1–7] and therefore provide a novel type of biomarker for various patient scenarios.

EVs are small membranous vesicles that differ in their cellular origin, abundance and biogenesis[8], and are naturally secreted by almost all cell types to transport bioactive molecules intercellularly. EVs are positive for tetraspanin family proteins, such as CD63, CD81 and CD9 (refs 9–11), and contain cell surface proteins as well as both mRNA and microRNA[12]. Conventional methods of analyzing EVs generally require large quantities of EVs to be concentrated and processed via time-consuming immunoblotting or enzyme-linked immunosorbent assay (ELISA) assays; these methods are impractical in most clinical settings. In this study, we establish a highly sensitive and rapid analytical technique for profiling surface proteins in EVs from patient blood that can be used to identify biomarkers of colorectal cancer, named ExoScreen. ExoScreen could monitor circulating EVs in serum without the need for purification step. In addition, we show that ExoScreen is superior for the detection of EVs to conventional methods, immunoblotting and ELISA. Furthermore, we find that ExoScreen enables to detect CD147 and CD9 double-positive EVs, which is abundantly secreted from colorectal cancer cells, in serum from colorectal cancer patients. Our results demonstrate that ExoScreen can be a tool for detection of EVs from as little as 5 μl of cancer patients' serum to detect circulating cancer-derived EVs.

Results

Establishment of ExoScreen to detect EVs in serum. To realize the usage of EVs in clinical situation, we develop methods that specifically detect circulating EVs in the serum based on an amplified luminescent proximity homogeneous assay using photosensitizer-beads[13] without a purification step of EVs

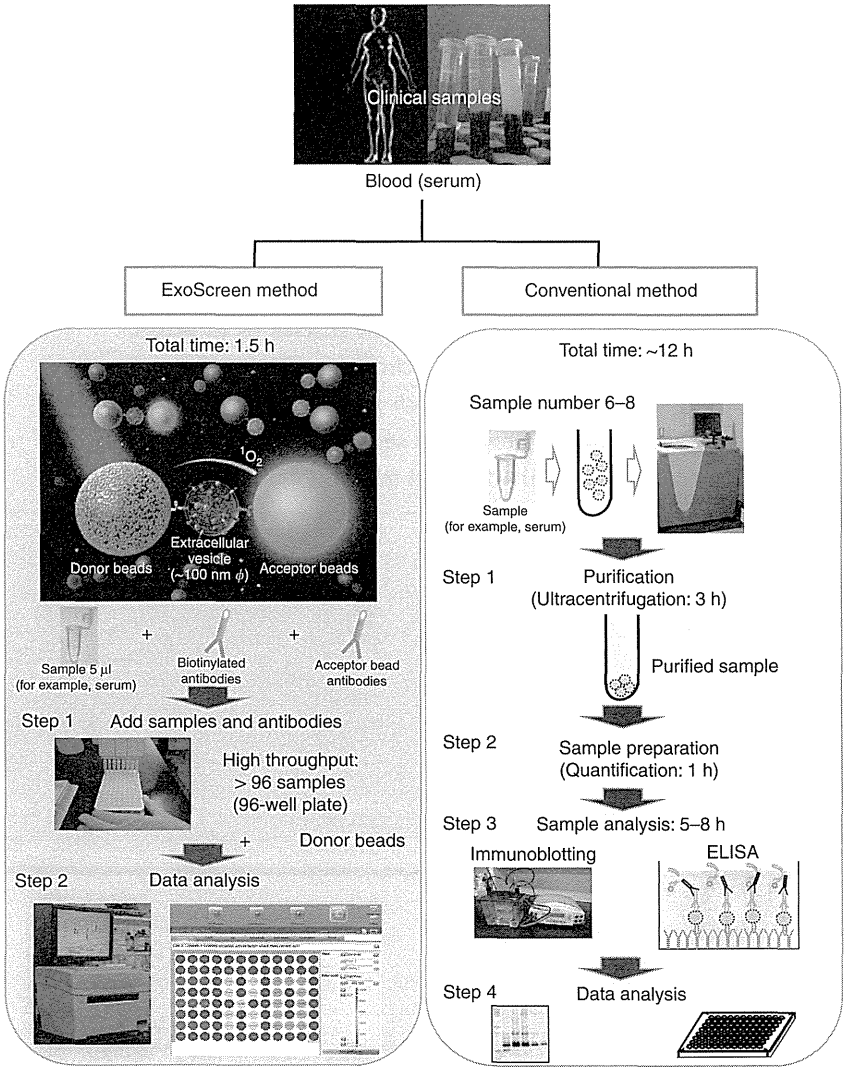

Figure 1 | Schematic overview depicting the method for detecting circulating EVs via conventional methods and ExoScreen. In the case of conventional methods, nearly 12 h are needed to detect the expression of certain protein in circulating EVs. In addition, excessive volumes of serum are required. Conversely, ExoScreen is completed within 2 h and requires only 5 μl of serum. In this system, streptavidin-coated donor beads capture an analyte-specific biotinylated antibody and are used in conjunction with acceptor beads conjugated to a second antibody. The streptavidin-coated donor beads are excited with a laser at 680 nm, resulting in the release of singlet oxygen, which excites an amplified fluorescent signal in the acceptor bead that emits at 615 nm when the beads are within 200 nm of the captured analyte.

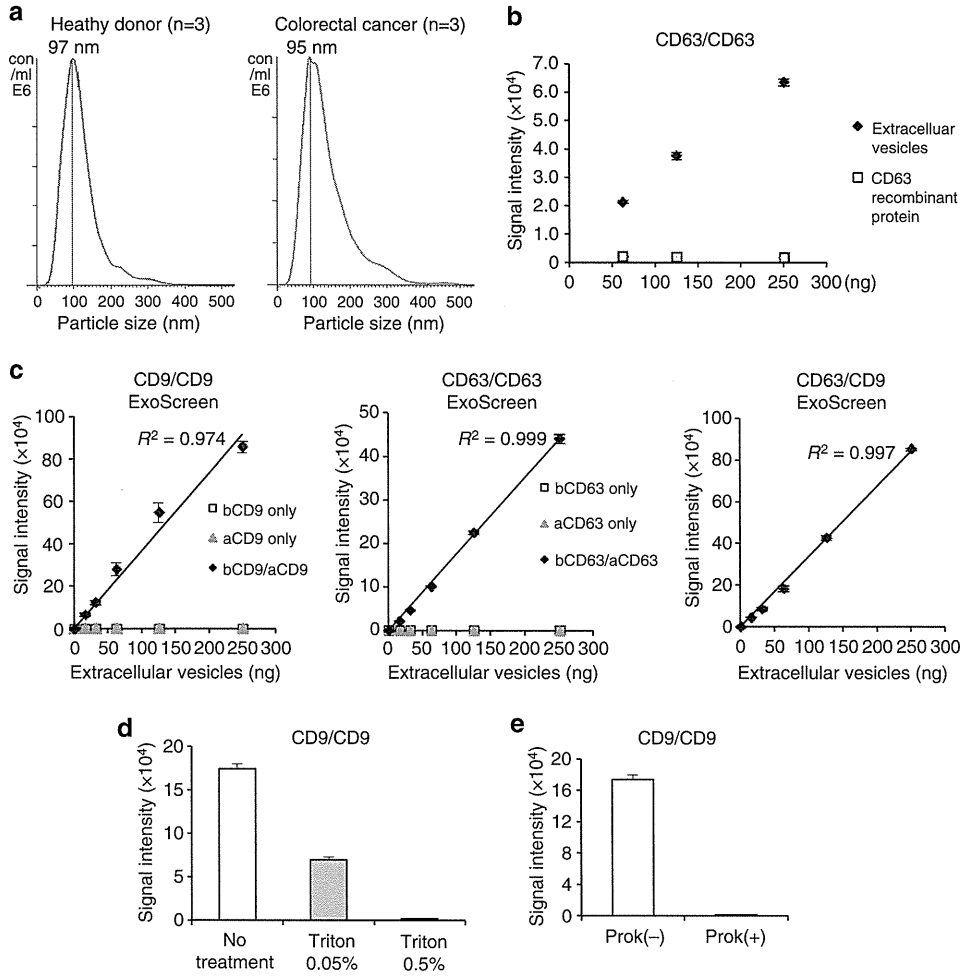

Figure 2 | Establishment of ExoScreen to detect the EVs. (**a**) Analysis of the size distribution in the serum of healthy donors ($n=3$) and colorectal cancer patients ($n=3$) by the NanoSight nanoparticle tracking system. (**b**) Detection of EVs or monomeric recombinant CD63 protein by ExoScreen using a CD63 antibody. EV protein concentration was measured via the Qubit system. The concentration of recombinant CD63 was adjusted with that of protein in EVs purified from HCT116 CM. Error bars are s.e.m. ($n=3$ for each condition). (**c**) Correlation between ExoScreen measurements for CD9 positive EVs, CD63 positive EVs or CD63/CD9 double-positive EVs and EV protein concentration in a dilution series. EV protein concentration was measured via the Qubit system. EVs were purified from HCT116 cell CM. The addition of biotinylated CD9 or CD63 antibodies without acceptor beads conjugated to antibodies is denoted 'bCD9 only' or 'bCD63 only', while 'aCD9 only' or 'aCD63 only' means addition of only acceptor beads conjugated to CD9 or CD63 antibodies without biotinylated antibodies. The addition of biotinylated antibodies and acceptor beads conjugated antibodies is denoted 'bCD9/aCD9' or 'bCD63/aCD63'. Right panel shows the addition of biotinylated CD63 antibodies and acceptor beads conjugated CD9 antibodies. Error bars are s.e.m. ($n=3$ for each condition). (**d**) Evaluation of ExoScreen specificity against purified EVs from HCT116 cell treated with or without 0.05% and 0.5% Triton X-100. Two hundred fifty ng of EVs were detected by ExoScreen using CD9 antibodies. Error bars are s.e.m. ($n=3$ for each condition). (**e**) Evaluation of ExoScreen specificity against EVs from HCT116 cells treated with (Prok(+)) or without (Prok(−)) Proteinase K. Two hundred fifty ng of EVs were detected by ExoScreen using CD9 antibodies. Error bars are s.e.m. ($n=3$ for each condition). Data are representative of at least three independent experiments each.

(Fig. 1). This system utilizes streptavidin-coated donor beads to capture an analyte-specific biotinylated antibody, and acceptor beads conjugated to a second antibody that recognizes an epitope of the analyte. The donor beads are excited with a laser at 680 nm, resulting in the release of singlet oxygen, which excites an amplified fluorescent signal in the acceptor beads. As a result, the acceptor beads emit light at 615 nm, but only if they are within 200 nm of the analyte captured by both antibodies. As shown in Fig. 2a, the size of EVs measured by the Nanosight particle tracking system was approximately 100 nm, which prevented the detection of larger vesicles, such as apoptotic bodies, shedding vesicles or protein complexes. In addition, we could not obtain signals from CD63 recombinant protein by ExoScreen, indicating that this assay does not detect antigen monomers (Fig. 2b). We call this assay 'ExoScreen' because the target of the assay is EVs and because it has a possibility to screen for biomarker of various diseases.

To confirm the reliability for detecting EVs by ExoScreen, we selected CD9 and CD63, which are abundant on the surface of EVs and are expressed in numerous cells, to detect EVs. Conditioned medium (CM) of prostate cancer, prostate epithelial, breast cancer and colorectal cancer cell lines were processed to obtain purified EVs. ExoScreen was able to quantify the amount of EVs present in cell culture supernatants with CD9 and CD63 positive EVs detectable in a dose-dependent manner (Fig. 2c and Supplementary Fig. 1). The negative controls, represented by only the biotinylated antibody or acceptor bead-conjugated antibody, resulted in a minimal fluorescent signal (Fig. 2c). In addition, the signal was decreased after detergent treatment (Fig. 2d and Supplementary Fig. 2) or Proteinase K treatment (Fig. 2e and

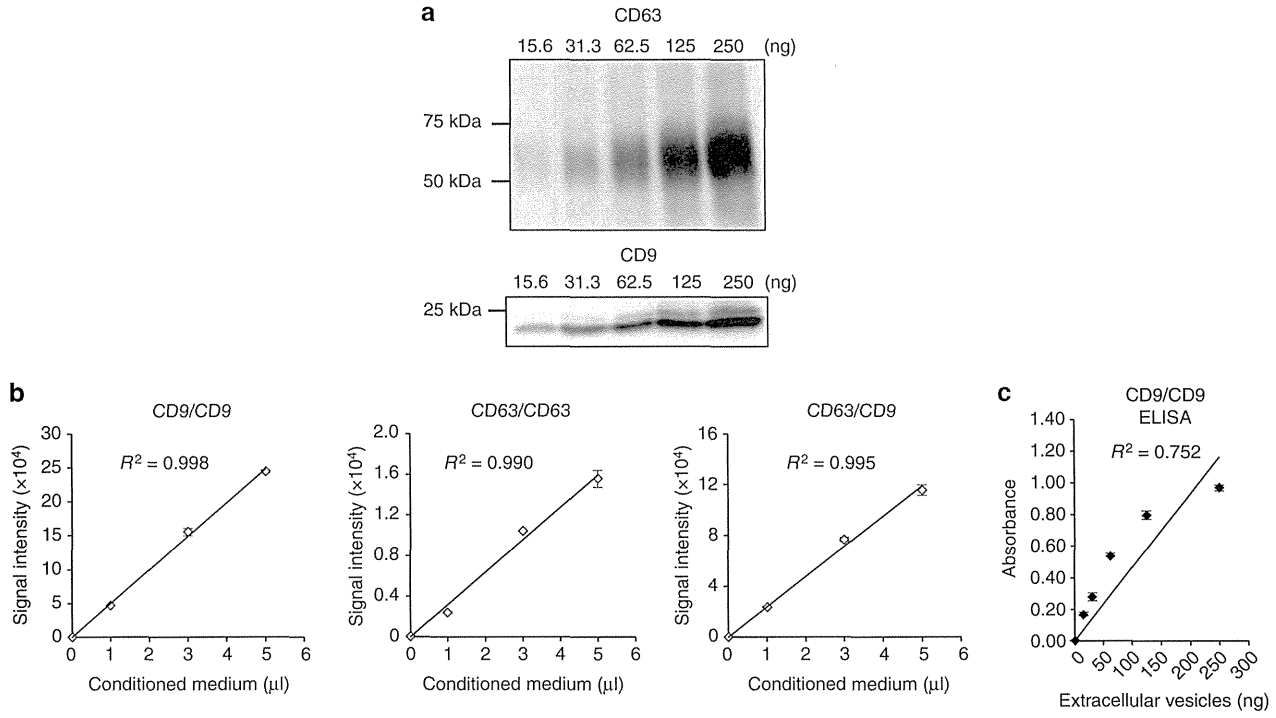

Figure 3 | Comparison of ExoScreen and conventional methods. (**a**) Immunoblotting analysis of CD63 (upper panels) or CD9 (lower panels) against the EVs isolated from HCT116 cells. EV protein concentration were measured via the Qubit system. EVs were purified from HCT116 cell CM. (**b**) Correlation between ExoScreen measurements for CD9 positive, CD63 positive or CD63/CD9 double-positive EVs and HCT116 cell CM in a dilution series. CM was prepared for 5 μl and diluted as indicated. Error bars are s.e.m. ($n=3$ for each condition). (**c**) Correlation between ELISA measurements for CD9 positive EVs and EV protein concentration in a dilution series. EV protein concentration were measured via the Qubit system. EVs were purified from HCT116 cell CM. Error bars are s.e.m. ($n=3$ for each condition). Data are representative of at least three independent experiments each.

Table 1 | Comparison of ExoScreen and ELISA.

	ExoScreen	ELISA
Incubation time	1.5-3 h	3-6 h + coating time
Steps	2	More than 5
Washes	No	Yes
Throughput	High	Low
Sample volume	Less than 5 μl*	50-200 μl†
The volume of antibodies	Low	High
Dynamic range	3-4 logs	2 logs
Analytic range‡	3 orders of magnitude	2 orders of magnitude
Sensitivity	High	High
Plate format	96-well or 384-well	96-well

ELISA, enzyme-linked immunosorbent assay.
*Total assay volume 50 μl.
†Total assay volume 200 μl.
‡Calculated by CD9/CD9 analysis of EVs derived from HCT116 cells

Supplementary Fig. 3), indicating that ExoScreen detected complexes of membranous vesicle and transmembrane proteins. Immunoblotting of the same purified EVs preparations confirmed the data obtained by ExoScreen. In fact, CD9 and CD63 proteins were detectable via immunoblotting (Fig. 3a and Supplementary Fig. 4). As shown in Fig. 3a, approximately 32 ng of EV proteins were needed to properly detect CD63 by immunoblotting, while ExoScreen could detect 15.6 ng of purified EVs (Fig. 2c). Furthermore, EVs from only 1 μl of culture medium are enough to detect by ExoScreen (Fig. 3b and Supplementary Fig. 5). In addition, ExoScreen has a wide working range compared with ELISA (Figs 2c and 3c). Moreover, because ExoScreen is a mix-and-read assay, these conventional methods require many steps and substantial time compared with ExoScreen (Fig. 1). Thus, the ExoScreen assay increases throughput while substantially decreasing hands-on. Taken together, these results indicate that ExoScreen is superior for the detection of EVs to conventional immunoblotting and ELISA (Table 1). The results of EVs detection in culture supernatant without purification (Fig. 3b, Supplementary Figs 5 and 6) prompted us to investigate whether ExoScreen could detect and characterize EVs in human serum. To develop ExoScreen as a diagnostic tool for clinical use, we optimized the method to detect EVs in serum without purification because the protocol exhibited non-linearity of ExoScreen signals against serum samples (Fig. 4a). This non-linearity is most likely a result of the aggregation of condensed proteins in serum. Indeed, we added dextran-500 to suppress serum protein aggregation, and this

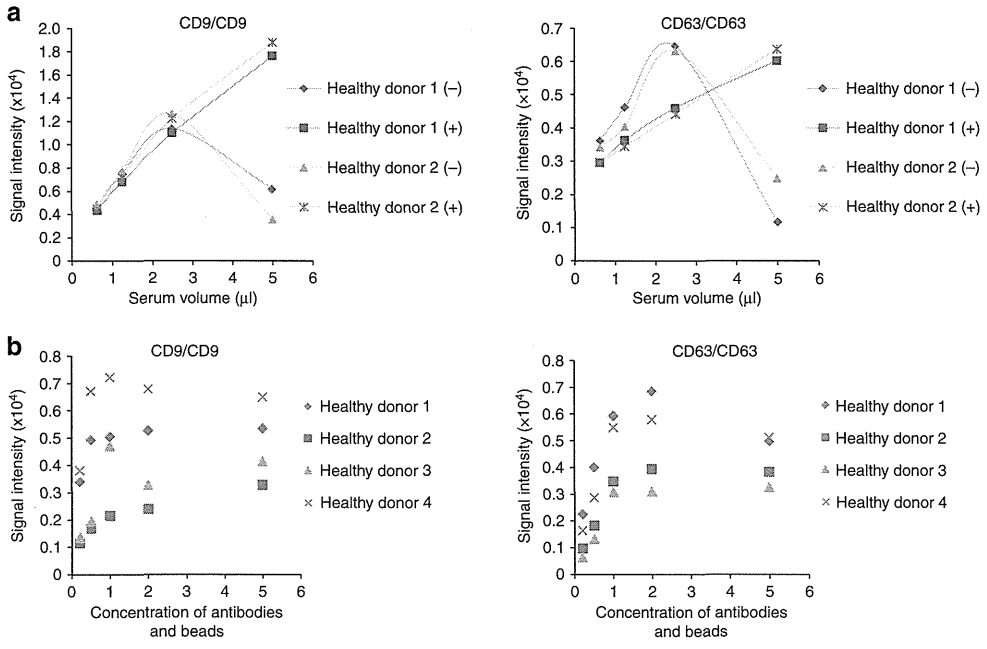

Figure 4 | Detection of circulating EVs in healthy donor sera. (**a**) Correlation between ExoScreen measurements for CD9 or CD63 and serum volume in a dilution series with (+) or without (−) Dextran-500. The final concentration of Dextran-500 was 1 mg ml^{-1}. (**b**) Concentration of '1' means the original concentration of donor and acceptor beads which we used in this study (see Methods section). In addition to original concentration, increased (twofold and fivefold) and decreased (0.5-fold and 0.25-fold) amount of donor and acceptor beads were evaluated by ExoScreen using serum from four healthy donors. Data are representative of at least three independent experiments each.

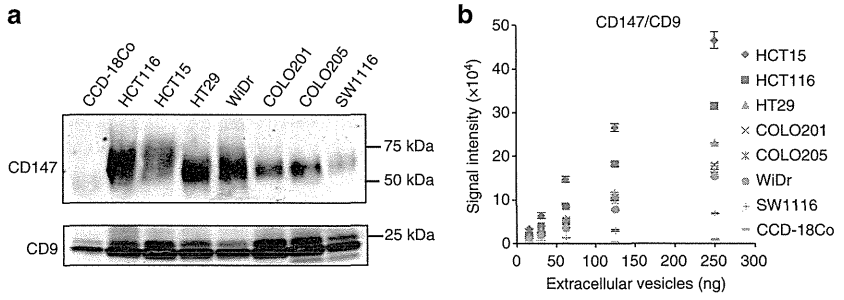

Figure 5 | Analysis of the amount of CD147 in EVs derived from various colon cancer cell lines and a normal colon fibroblast cell line. (**a**) Immunoblotting analysis of CD147 or CD9 against purified EVs isolated from CCD-18Co cells, HCT116 cells, HCT15 cells, HT29 cells, WiDr cells, COLO201 cells, COLO205 cells and SW1116 cells. EV proteins (250 ng) was used for the detection of CD147 and CD9. (**b**) Correlation between ExoScreen detection of CD147/CD9 double-positive EVs and EV protein concentration in a dilution series. EVs protein concentration was measured via the Qubit system. EVs were purified from CCD-18Co, HCT116, HCT15, HT29, WiDr, COLO201, COLO205 or SW1116 CM. Error bars are s.e.m. ($n=3$ for each condition). Data are representative of at least three independent experiments each.

treatment eliminated the disruption of signals by protein aggregation (Fig. 4a). As shown in Fig. 4a, ExoScreen revealed that serum EVs were captured and expressed both CD9 and CD63 without purification. Further, these signals were detectable in a dose-dependent manner (Fig. 4a). In addition, we assessed whether the concentration of beads, which we employed in this study, was appropriate for the detection of circulating EVs in serum by checking the various concentrations of beads via ExoScreen, and found that the concentration of beads we employed in this study was adequate (Fig. 4b). Taken together, these results indicated that ExoScreen could monitor circulating EVs in serum without the need for a purification process.

Enrichment of CD147 on EVs from colorectal cancer cell lines. Because EVs are known to represent an important and specific route of intercellular communication[14], we reasoned that tumour-derived EVs may differ from circulating EVs in normal physiological conditions. Previous reports showed that the protein components of EVs from cancer cells were different from normal cells[15,16]. Indeed, it has been recently reported that for patients with stage III melanoma, the amount of specific protein in EVs was significantly increased in individuals who eventually developed metastatic disease, indicating that EVs might have great potential for cancer diagnosis[6]. To identify cancer-derived EVs in cancer patients, EVs derived from the colorectal cancer cell line HCT116 cells and a normal colon fibroblast cell line CCD-18Co cells were subjected to proteomic analysis (Supplementary Table 1). When EVs isolated from CCD-18Co cells were compared with HCT116 cells, the amount of CD147, which is the immunoglobulin superfamily member, was found to be significantly high in the EVs of HCT116 cells, whereas the expression could not be observed in CCD-18Co cells.

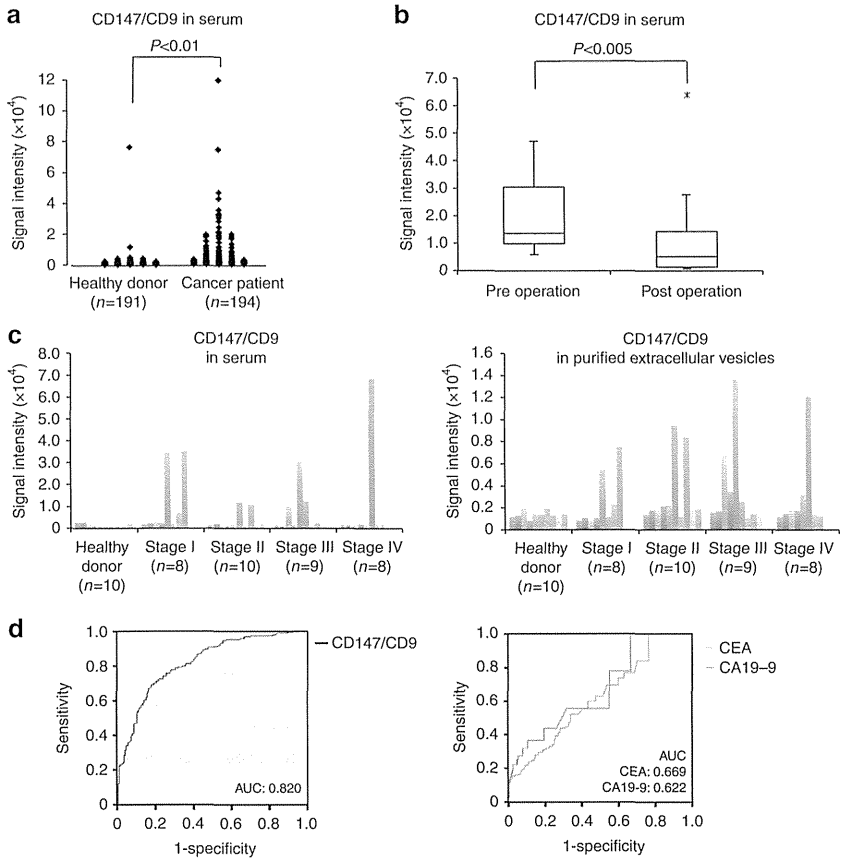

Figure 6 | Analysis of circulating CD147 and CD9 double-positive EVs in healthy donors or colorectal cancer patient sera. (**a**) Serum levels of CD147/CD9 double-positive EVs in colorectal cancer patients without any purification. The panel shows a scatter plot for healthy donors ($n=191$) and colorectal cancer patients ($n=194$). The *P*-value was calculated by using Wilcoxon rank-sum test. (**b**) Changes in serum levels of CD147/CD9 double-positive EVs in colorectal cancer patients (stage I or II: $n=15$) before (preoperation) and after (postoperation after 7–34 days) surgical removal of the tumor. Box lengths represent the interquartile range (first to third quartiles). The line in the center of the boxes represents the median value. Data represented by the asterisks are extreme values (greater than three times the interquartile range over the third quartile). The *P*-value was calculated by using Wilcoxon signed-rank test. (**c**) The results of ExoScreen detection of circulating EVs (left panel) and purified circulating EVs (right panel) in sera from healthy donors ($n=10$) and colorectal cancer patients ($n=35$) using CD147 and CD9 antibodies. The panels show the signal intensities from each samples measured for CD147/CD9 double-positive EVs using ExoScreen. (**d**) Receiver operating characteristic curves between healthy donors and colorectal cancer patients assesing by CD147/CD9 double-positive EVs (left panel), CEA and CA19-9 (right panel). left panel, CD147/CD9 double-positive EVs (healthy donors versus colorectal cancer patients; AUC: 0.820); right panel, CEA (AUC: 0.669); CA19-9 (AUC: 0.622) Data are representative of at least three independent experiments each. AUC, area under the curve.

Notably, CD147 is plasma membrane protein and this is suitable for applying to the ExoScreen. We observed that CD147 is expressed on all of the colorectal cancer cell lines, but their expression levels are not uniform (Fig. 5a,b and Supplementary Figs 7 and 8). In addition, CD147 in EVs from CCD-18Co cells was hardly detectable. Several reports have shown that CD147 is expressed in the majority of human tumour types including colorectal cancer[17,18], although CD147 is expressed in a variety of embryonic and adult tissues, such as spermatocytes, neuronal cells, erythrocyte and so on[19]. In addition, CD147 functions in lactate transporter, which is an important feature of cancer cell, because of the excessive anaerobic glycolysis phenomenon in cancer cells referred to as the Warburg effect[20]. Indeed, associations between high expression of CD147 and poor prognosis have previously been shown in colorectal cancer[21], thus representing a potential marker for *ex vivo* analysis of tumour-derived EVs.

CD147 and CD9 double-positive EVs in clinical samples. Next, we used ExoScreen to detect cancer-derived EVs in human clinical samples (Fig. 6a). As shown in Fig. 6a, we found that CD147 and CD9 double-positive EVs were significantly higher in serum from cancer patients ($n=194$) than in serum from healthy donors ($n=191$). Most importantly, most of CD147 in cancer patient sera reduced after surgery (Fig. 6b), suggesting that the reduced signal of CD147 obtained from ExoScreen is originated from cancer-derived EVs, even the variety of cells expressed CD147. To confirm whether by ExoScreen really reflects the protein profile of EVs in circulation, EVs were purified from the sera of tumour patients ($n=35$) and healthy donors ($n=10$) and analysed for expression of CD147 via immunoblotting (Supplementary Fig. 9). We also performed ExoScreen against the same serum samples obtained by ultracentrifugation (Fig. 6c, right panel). As depicted in Supplementary Fig. 9, the expression of CD147 in EVs isolated from the sera of cancer patients correlated clearly with the results obtained from the ExoScreen assay (Fig. 6c), indicating that the accuracy of ExoScreen was confirmed and that it can be used to monitor EVs in circulation without any purification. Taken together, these results demonstrate that ExoScreen can be a tool for detection of EVs from as little as 5 μl of cancer patients' serum to detect circulating cancer-derived EVs.

Discussion

In summary, we propose a rapid, highly sensitive and widely usable detection method based on the amplified luminescent proximity homogeneous assay using photosensitizer-beads for cancer cell-derived EVs. Notably, different antibodies can be conjugated to capture different analytes, such as CD147, thus various types of cancer can be targetd. There are various colorectal cancer screening tests. For example, the fecal occult blood test has been recommended widely as a screening test for colorectal cancer; however, the fecal occult blood displays low sensitivity and specificity for detecting colorectal cancer[22]. Moreover, carcinoembrionic antigen (CEA) and carbohydrate antigen 19-9 (CA19-9) are the most commonly used tumour-associated antigens in the management of patients with colorectal cancer, although those biomarkers are not sensitive enough for early colorectal cancer[23,24]. In fact, the high levels of CD147 detected in patient sera showed the normal value range of CEA and CA19-9 in stage I patients (Supplementary Tables 2 and 3). In addition, the receiver operating characteristic curve indicates a diagnostic advantage of CD147/CD9 double-positive EVs in comparison with CEA and CA19-9 (Fig. 6d). From these aspects and the result shown in Fig. 6b, ExoScreen detecting CD147/CD9 double-positive EVs might be used for monitoring the status of cancer after the surgery and during chemotherapy, resulting in increase in QOL of the patients and providing doctor for the proper assessment of patient status. Further studies are needed to know whether our ExoScreen reduces colorectal cancer mortality as a screening test. It should be noted that CD147/CD9 double-positive EVs were also detected in samples with early stage colorectal cancer that invade into submucosal layer (T1 stage according to UICC classification) (Supplementary Table 2) by the ExoScreen assay. These results also indicate that ExoScreen can be used to detect biomarkers for diseases that are currently difficult to diagnose and monitor not only cancer, but autoimmune disease and degenerative disease of the brain. Thus, our data suggest that ExoScreen, in addition to being a novel liquid biopsy platform for the detection of circulating EVs, may aid variety of disease diagnosis and help to identify companion biomarkers that are important for new drug development.

Methods

Cell cultures. Human colorectal cancer cell lines (HCT116 cells, HCT15 cells, HT29 cells, COLO201 cells, COLO205 cells, WiDr cells and SW1116 cells) and normal colon fibroblast cell line CCD-18Co cells were purchased from American Type Culture Collection. HCT116 and HT29 cells were cultured in McCoy's 5A medium supplemented with 10% heat-inactivated fetal bovine serum (FBS) and an antibiotic–antimycotic solution (Invitrogen) at 37 °C in 5% CO_2. WiDr cells CCD-18Co cells were cultured in minimal essential medium (MEM) containing 2 mM L-gulutamine, an antibiotic–antimycotic solution, nonessential amino acids and 10% FBS at 37 °C in 5% CO_2. HCT15 cells, COLO201 cells and COLO205 cells were cultured in RPMI 1640 medium supplemented with 10% heat-inactivated FBS and an antibiotic–antimycotic solution at 37 °C in 5% CO_2. SW1116 cells were cultured in Leibovitz' L15 medium supplemented with 10% heat-inactivated FBS and an antibiotic–antimycotic solution at 37 °C in without CO_2. The following additional cell lines were used: PNT2 cells, an immortalized normal adult prostatic epithelial cell line (DS Pharma Biomedical Co., Ltd. Osaka, Japan); PC3 cells, a human prostate cancer cell line initiated from a bone metastasis of a grade IV prostatic adenocarcinoma (American Type Culture Collection); MDA-MB-231-luc-D3H2LN cells (MDA-MB-231LN), a highly metastatic human breast cancer cell line (Xenogen); and MCF7 cells, a human breast cancer cell line which expresses oestrogen receptor (American Type Culture Collection). The above cells were cultured in RPMI 1640 medium supplemented with 10% FBS and an antibiotic–antimycotic solution at 37 °C in 5% CO_2.

Patient serum samples. Collection and usage of human serum from corolectal cancer patients ($n = 194$) and healthy donor ($n = 94$) were approved by Osaka university Institutional Review Board (No.11343). Serum was aliquoted and kept at − 80 °C until used, and freeze-thawing was avoided as much as possible after that. Some part of the serum samples ($n = 97$) from healthy donor shown in Fig. 6a were purchased from BizCom Japan (Tokyo, Japan). Serum samples containing red blood cells were excluded from the analysis. Informed consent was obtained from all patients.

Preparation of conditioned media and EVs. The cells were washed with phosphate-buffered saline (PBS), and the culture medium was replaced with advanced Dulbecco's Modified Eagle Medium for HCT116 cells, WiDr cells, SW1116 cells, HT29 cells and CCD-18Co cells, or advanced RPMI medium for the other cell lines, containing an antibiotic–antimycotic and 2 mM L-glutamine (but not containing FBS). After incubation for 48 h, the CM was collected and centrifuged at 2,000 *g* for 10 min at 4 °C. To thoroughly remove cellular debris, the supernatant was filtered through a 0.22 μm filter (Millipore). The CM was then used for EV isolation. To prepare EVs, CM or the sera from colorectal patients and healthy donors were ultracentrifuged at 110,000 *g* for 70 min at 4 °C. The pellets were washed with 11 ml of PBS, ultracentrifuged at 110,000 *g* for 70 min at 4 °C and resuspended in PBS. The putative EVs fraction was measured for its protein content using a Quant-iT Protein Assay with Qubit2.0 Fluorometer (Invitrogen).

Reagents. The following antibodies were used for immunoblotting: mouse monoclonal anti-human CD63 antibody (clone H5C6, dilution 1:200) from BD Biosciences, mouse monoclonal anti-human CD9 antibody (clone ALB 6, dilution 1:200) from SantaCruz Biotechnology, mouse monoclonal anti-human CD147 antibody (clone MEM-M6/1, dilution 1:1,000) from Novus Biologicals and mouse monoclonal anti-Actin (clone C4, dilution 1:1,000) from Millipore. The secondary antibody (horseradish peroxidase-labeled sheep anti-mouse) were purchased from GE HealthCare.

The following antibodies used for ExoScreen and ELISA were developed in Shionogi & Co., LTD.: mouse monoclonal anti-human CD63 antibody (clone 8A12) and mouse monoclonal anti-human CD9 antibody (clone 12A12). Mouse monoclonal anti-human CD147 antibody (clone MEM-M6/1) was purchased from Novus Biologicals. Antibodies were used to modify either acceptor bead or biotin following the manufacturer's protocol.

AlphaLISA reagents (Perkin Elmer, Inc., Waltham, MA 02451, USA) consisted of AlphaScreen Streptavidin-coated donor beads (6760002), AlphaLISA Unconjugated-acceptor beads (6062011) and AlphaLISA Universal buffer (AL001F). AlphaLISA assays were performed in 96-well half-area white plates (6005560) and read in an EnSpire Alpha 2300 Multilabel Plate reader (Perkin Elmer, Inc.).

ExoScreen assay. A 96-well half-area white plate was filled with 5 μl of sample, 5 nM biotinylated antibodies and 50 μg ml^{-1} AlphaLISA acceptor beads conjugated antibodies in the universal buffer. The volume of each reagent was 10 μl. The plate was then incubated for 1–3 h at room temperature. Without a washing step, 25 μl of 80 μg ml^{-1} AlphaScreen streptavidin-coated donor beads were added. The reaction mixture was incubated in the dark for another 30 min at room temperature and the plate was then read on the EnSpire Alpha 2300 Multilabel Plate reader using an excitation wavelength of 680 nm and emission detection set at 615 nm. Background signals obtained from PBS were subtracted from the measured signals.

ELISA. Ninety-six well-plates (Nunc) were coated with 2.5 μg ml^{-1} anti-human CD9 or -CD63 antibodies in a volume of 50 μl per well of carbonate buffer (pH 9.6) and incubated for 4 h at room temperature. After 2 washes with 0.01% Tween-20 in PBS, 100 μl per well of Blocking One solution (Nacalai Tesque) was added at room temperature for 1 h. Following 3 washes in PBS, EVs purified from cell culture supernatants were added in a final volume of 50 μl and incubated for 1 h at room temperature. After 3 washes with PBS, 50 μl of biotinylated anti-human CD9 or -CD63 antibodies diluted to 1 μg ml^{-1} were added and incubated for 1 h at room temperature. After 3 washes with PBS, the plate was incubated with 100 μl of HRP-conjugated streptavidin (Cell Signalling Technology) diluted 1:2,000 in Blocking One solution for 1 h at room temperature. After the final 3 washes with PBS, the reaction was developed with Peroxidase (TMB One Component HRP Microwell Substrate, SurModics). The reaction was arrested with 450 nm Stop Reagent for TMB Microwell Substrates (SurModics) and optical densities were recorded at 450 nm.

Immunoblotting. Equal amounts of EVs or whole-cell lysates were loaded onto 4–15% Mini-PROTEAN TGX gels (Bio-Rad, Munich, Germany). Following electrophoresis (100 V, 30 mA), the proteins were transferred to a polyvinylidene difluoride membrane. The membranes were blocked with Blocking One solution and then incubated with primary antibodies. After washing, the membranes were incubated with horseradish peroxidase-conjugated sheep anti-mouse IgG and then subjected to enhanced chemiluminescence using ImmunoStar LD (Wako). CD63, CD9 and CD147 were detected under non-reducing conditions. Original scans of the cropped images in the main figures (Figs 3a and 5a) are presented in Supplementary Fig. 10.

Measurement of size distribution by NTA. Nanoparticle tracking analysis (NTA) was carried out using the Nanosight system (NanoSight) on sera diluted 1000-fold with PBS for analysis. The system focuses a laser beam through a suspension of the particles of interest. These are visualized by light scattering using a conventional optical microscope aligned perpendicularly to the beam axis, which collects light scattered from every particle in the field of view. A 60 s video recorded all events for further analysis by NTA software. The Brownian motion of each particle was tracked between frames to calculate its size using the Stokes–Einstein equation.

References

1. Iero, M. *et al.* Tumour-released exosomes and their implications in cancer immunity. *Cell Death Differ.* **15,** 80–88 (2008).
2. Webber, J., Steadman, R., Mason, M. D., Tabi, Z. & Clayton, A. Cancer exosomes trigger fibroblast to myofibroblast differentiation. *Cancer Res.* **70,** 9621–9630 (2010).
3. Al-Nedawi, K. *et al.* Intercellular transfer of the oncogenic receptor EGFRvIII by microvesicles derived from tumour cells. *Nat. Cell Biol.* **10,** 619–624 (2008).
4. Skog, J. *et al.* Glioblastoma microvesicles transport RNA and proteins that promote tumour growth and provide diagnostic biomarkers. *Nat. Cell Biol.* **10,** 1470–1476 (2008).
5. Taylor, D. D. & Gercel-Taylor, C. MicroRNA signatures of tumor-derived exosomes as diagnostic biomarkers of ovarian cancer. *Gynecol. Oncol.* **110,** 13–21 (2008).
6. Peinado, H. *et al.* Melanoma exosomes educate bone marrow progenitor cells toward a pro-metastatic phenotype through MET. *Nat. Med.* **18,** 883–891 (2012).
7. Kosaka, N., Iguchi, H. & Ochiya, T. Circulating microRNA in body fluid: a new potential biomarker for cancer diagnosis and prognosis. *Cancer. Sci.* **101,** 2087–2092 (2010).
8. Raposo, G. & Stoorvogel, W. Extracellular vesicles: exosomes, microvesicles, and friends. *J. Cell Biol.* **200,** 373–383 (2013).
9. Mathivanan, S. & Simpson, R. J. ExoCarta: a compendium of exosomal proteins and RNA. *Proteomics* **9,** 4997–5000 (2009).
10. Bobrie, A. *et al.* Rab27a supports exosome-dependent and -independent mechanisms that modify the tumor microenvironment and can promote tumor progression. *Cancer Res.* **72,** 4920–4930 (2012).
11. Yoshioka, Y. *et al.* Comparative marker analysis of extracellular vesicles in different human cancer types. *J. Extracell. Vesicles* **2,** doi:10.3402/jev.v2i0.20424 (2013).
12. Valadi, H. *et al.* Exosome-mediated transfer of mRNAs and microRNAs is a novel mechanism of genetic exchange between cells. *Nat. Cell Biol.* **9,** 654–659 (2007).
13. Eglen, R. M. *et al.* The use of AlphaScreen technology in HTS: current status. *Curr. Chem. Genomics* **25,** 2–10 (2008).
14. Kosaka, N. *et al.* Neutral sphingomyelinase 2 (nSMase2)-dependent exosomal transfer of angiogenic microRNAs regulate cancer cell metastasis. *J. Biol. Chem.* **288,** 10849–10859 (2013).
15. Xiao, D. *et al.* Identifying mRNA, microRNA and protein profiles of melanoma exosomes. *PLoS One* **7,** e46874 (2012).
16. Choi, D. S. *et al.* Quantitative proteomics of extracellular vesicles derived from human primary and metastatic colorectal cancer cells. *J. Extracell. Vesicles* **1,** doi:10.3402/jev.v1i0.18704 (2012).
17. Riethdorf, S. *et al.* High incidence of EMMPRIN expression in human tumors. *Int. J. Cancer.* **119,** 1800–1810 (2006).
18. Li, Y. *et al.* HAb18G (CD147), a cancer-associated biomarker and its role in cancer detection. *Histopathology* **54,** 677–687 (2009).
19. Muramatsu, T. & Miyauchi, T. Basigin (CD147): a multifunctional transmembrane protein involved in reproduction, neural function, inflammation and tumor invasion. *Histol. Histopathol.* **18,** 981–987 (2003).
20. Weidle, U. H., Scheuer, W., Eggle, D., Klostermann, S. & Stockinger, H. Cancer-related issues of CD147. *Cancer. Genomics. Proteomics.* **7,** 157–169 (2010).
21. Boye, K. *et al.* EMMPRIN is associated with S100A4 and predicts patient outcome in colorectal cancer. *Br. J. Cancer.* **107,** 667–674 (2012).
22. Ahlquist, D. A. *et al.* Accuracy of fecal occult blood screening for colorectal neoplasia. A prospective study using Hemoccult and HemoQuant tests. *JAMA* **269,** 1262–1267 (1993).
23. Chapman, M. A., Buckley, D., Henson, D. B. & Armitage, N. C. Preoperative carcinoembryonic antigen is related to tumour stage and long-term survival in colorectal cancer. *Br. J. Cancer.* **78,** 1346–1349 (1998).
24. Kuusela, P. *et al.* Comparison of CA 19-9 and carcinoembryonic antigen (CEA) levels in the serum of patients with colorectal diseases. *Br. J. Cancer.* **49,** 135–139 (1984).

Acknowledgements

This work was supported in part by a Grant-in-Aid for the Third-Term Comprehensive 10-Year Strategy for Cancer Control, a Grant-in-Aid for Scientific Research on Priority Areas Cancer from the Ministry of Education, Culture, Sports, Science and Technology, and the Program for Promotion of Fundamental Studies in Health Sciences of the National Institute of Biomedical Innovation (NiBio), and the Japan Society for the Promotion of Science (JSPS) through the 'Funding Program for World-Leading Innovative R&D on Science and Technology (FIRST Program)' initiated by the Council for Science and Technology Policy (CSTP), and a Grant-in-aid for Project for Development of Innovative Research on Cancer Therapeutics (P-Direct), and Grant-in-Aid for Scientific Research on Innovative Areas ('functional machinery for non-coding RNAs') from the Japanese Ministry of Education, Culture, Sports, Science, and Technology, and Comprehensive Research and Development of a Surgical Instrument for Early Detection and Rapid Curing of Cancer Project (P10003) of the New Energy and IndustrialTechnology Development Organization (NEDO), a research program of the Project for Development of Innovative Research on Cancer Therapeutics (P-Direct), Ministry of Education, Culture, Sports, Science and Technology of Japan. We thank Ms. Ayako Irie at Quantum design Japan for supporting the Nanosight tracking analysis. We thank Ms. Ayako Inoue for excellent technical assistance. We thank Dr Roger Bosse and Dr Nami Kamura at Perkin Elmer for advising protocol for AlphaLisa system.

Author contributions

T.O. originated the concept. Y.Y., N.K. and T.O. carried out the project design. H.Oh., H.Ok. and H.S. developed the antibodies. R.N., H.Y., H.I., M.M., K.F. and T.N provided the serum samples. H.Ha., H.S., H.Hi., F.T. and T.K. assisted with data interpretation. Y.K. and Y.Y. performed the experiments and T.O. supervised the project; Y.Y., N.K. and T.O. contributed to the writing of the manuscript.

Additional information

Supplementary Information accompanies this paper at http://www.nature.com/naturecommunications

Competing financial interests: The authors declare no competing financial interests.

Reprints and permission information is available online at http://npg.nature.com/reprintsandpermissions/

How to cite this article: Yoshioka, Y. *et al.* Ultra-sensitive liquid biopsy of circulating extracellular vesicles using ExoScreen. *Nat. Commun.* 5:3591 doi: 10.1038/ncomms4591 (2014).

FULL PAPER

BJC

British Journal of Cancer (2014), 1–9 | doi: 10.1038/bjc.2014.289

Keywords: CD10; head and neck squamous cell carcinoma; cell surface antigen array; chemo-resistance; radio-resistance; cancer stem cells

CD10 as a novel marker of therapeutic resistance and cancer stem cells in head and neck squamous cell carcinoma

T Fukusumi[1,2], H Ishii[2], M Konno[2], T Yasui[1], S Nakahara[1], Y Takenaka[1], Y Yamamoto[1], S Nishikawa[2], Y Kano[2], H Ogawa[3], S Hasegawa[3], A Hamabe[3], N Haraguchi[4], Y Doki[3], M Mori[3] and H Inohara*[,1]

[1]Department of Otorhinolaryngology—Head and Neck Surgery, Osaka University, Graduate School of Medicine, Suita, 2-2 Yamadaoka, Osaka 565-0871, Japan; [2]Department of Frontier Science for Cancer and Chemotherapy, Osaka University, Graduate School of Medicine, Suita, 2-2 Yamadaoka, Osaka 565-0871, Japan; [3]Department of Gastroenterological Surgery, Osaka University, Graduate School of Medicine, Suita, 2-2 Yamadaoka, Osaka 565-0871, Japan and [4]Department of Surgery, Osaka National Hospital, Osaka, Tyuou-ku, 2-1-14 Houenzaka, Osaka 540-0006, Japan

Background: Cancer stem cells (CSCs) are responsible for treatment failure. However, their identification and roles in resistance are not well established in head and neck squamous cell carcinoma (HNSCC).

Methods: Three HNSCC cell lines (FaDu, Detroit562 and BICR6) were treated with cisplatin or radiation. Cell surface antigens were analysed by LyoPlate, a novel cell surface antigen array. The expression levels of antigens highly expressed after treatments were further compared between cisplatin-resistant Detroit562 cells and its parental line. Association of the candidate antigen with CSCs properties, namely sphere formation and *in vivo* tumourigenicity, was also examined.

Results: CD10, CD15s, CD146 and CD282 were upregulated across the treated cell lines, while the increased expression of CD10 was prominent in the cisplatin-resistant cell line. Isolation mediated by FACS revealed that the CD10-positive subpopulation was more refractory to cisplatin, fluorouracil and radiation than the CD10-negative subpopulation. It also showed an increased ability to form spheres *in vitro* and tumours *in vivo*. Moreover, the CD10-positive subpopulation expressed the CSC marker *OCT3/4* at a higher level than that in the CD10-negative subpopulation.

Conclusions: CD10 is associated with therapeutic resistance and CSC-like properties of HNSCC. CD10 may serve as a target molecule in the treatment of refractory HNSCC.

Head and neck squamous cell carcinoma (HNSCC) is the sixth most common malignancy worldwide (Argiris *et al*, 2008). Despite recent advances in its diagnosis and management, long-term survival of patients with HNSCC remains poor (Lo *et al*, 2003). Radiotherapy and chemotherapy initially control tumour growth; however, over time many patients suffer relapse. To improve prognosis, the establishment of a novel marker to predict therapeutic resistance is required. This would also aid the optimisation of HNSCC treatment, and thus benefit patient outcome.

Cancer stem cells (CSCs) are defined as cells that possess the properties of tumour initiation and self-renewal. It is currently understood that CSCs are responsible for treatment failure in a diversity of cancers (Bao *et al*, 2006; Li *et al*, 2008). CD44 (Prince *et al*, 2007) and ALDH1 (Chen *et al*, 2009) have been reported to represent candidate markers of HNSCC CSCs; however, whether they serve as true markers remains controversial (Chen *et al*, 2011; Koukourakis *et al*, 2012). These discrepant reports prompted us to search for a novel marker specific to HNSCC CSCs. Thus, in the present study we aimed to identify a new cell surface antigen that is

*Correspondence: Professor H Inohara; E-mail: hinohara@ent.med.osaka-u.ac.jp

Revised 19 April 2014; accepted 1 May 2014

involved in therapeutic resistance, and to address whether it served as a marker for HNSCC CSCs. Through array analysis and testing of cell viability in the presence of therapeutic agents, we identified CD10 as a potential marker of refractory HNSCC. Moreover, CD10 was found to confer a CSC-like phenotype, and underscored expression of *OCT3/4*. Thus, CD10 could be a specific marker of HNSCC CSCs that contributes to therapeutic resistance.

MATERIALS AND METHODS

Cell culture. FaDu and Detroit562 cell lines were obtained from the ATCC (Manassas, VA, USA), while BICR6 was from ECACC (Proton Down, Salisbury, UK). FaDu and BICR6 were established from a primary hypopharyngeal cancer, while Detroit562 were from a lymph node metastasis of pharyngeal cancer. Cells were cultured in Dulbecco's modified Eagle's medium (DMEM; Sigma Aldrich, St. Louis, MO, USA) supplemented with 10% foetal bovine serum (FBS) and a penicillin ($50\,U\,ml^{-1}$) and streptomycin ($50\,\mu g\,ml^{-1}$) cocktail under an atmosphere of 5% CO_2 at 37 °C. The cisplatin-resistant Detroit562 cell line was established by continuous stepwise exposure to cisplatin starting from a concentration of 1 μM up to 10 μM.

Cell surface antigen arrays. Cells were exposed to 3 μM cisplatin for 7 days. Alternatively, cells were irradiated by a single fraction of 8 Gy and further cultured for 5 days. The expression patterns of cell surface antigens were then compared between the treated and untreated cells using the LyoPlate cell surface antigen array (BD Biosciences, San Jose, CA, USA). The kit consists of three 96-well plates coated with monoclonal antibodies along with AlexaFluor 647 conjugated goat anti-mouse Ig and goat anti-rat Ig secondary antibodies. It allows comprehensive analysis of 242 cell surface antigens by flow cytometry, which was performed using the Cell Analyzer EC800 (Sony, Tokyo, Japan).

Flow cytometry and cell sorting. Flow cytometry and cell sorting were performed using the FACSAria II (BD, Franklin Lakes, NJ, USA). Cells were harvested and single-cell suspensions were prepared with the aid of StemPro Accutase (Life Technologies, Carlsbad, CA, USA). Spheroid cells were separated into single-cell suspensions with the aid of collagenase I (Sigma Aldrich) and adjusted to a concentration of 10^7 cells ml^{-1}. To stain surface antigens, cells were incubated with antibodies against CD10, CD15s, CD44, CD146 and CD282 for 30 min on ice. The fluorophores for each antibody were as follows: CD10—Brilliant Violet (Biolegend, San Diego, CA, USA) and APC (BD Biosciences); CD44—FITC (BD Biosciences); CD146—APC (Biolegend); CD282—PE (BD Biosciences). For CD15s, we combined purified antibody (BD Biosciences) and the secondary antibody—APC/Cy7 (BD Biosciences). The antibodies against CD10, CD15s and the secondary antibody of CD15s were used at a concentration of $50\,\mu l\,ml^{-1}$. The antibodies against CD44, CD146 and CD282 were used at a concentration of $200\,\mu l\,ml^{-1}$. To stain ALDH1, we used the Aldefluor stem cell detection kit (StemCell Technologies, Vancouver, BC, Canada) at a concentration of $50\,\mu l\,ml^{-1}$ for 45 min at 37 °C. The fluorophore of Aldefluor was FITC. Doublet cells were eliminated using FSC-A/FSC-H and SSC-A/SSC-H. Dead and damaged cells were eliminated using 7-AAD (BD Biosciences). Briefly, after CD10, CD15s, CD44, CD146, CD282 and ALDH1 staining, 7-AAD was incubated with cells for 10 min at room temperature. Except cell sorting, all FACS analysis was performed three times.

Viability assay. Cells were seeded in 96-well plates at 3×10^3 cells per well, cultured overnight and then incubated with 0.1–5 μM cisplatin or 0.5–50 μM fluorouracil for 72 h. Alternatively, cells were irradiated at a single fraction of 8 Gy and then cultured for 72 h. Cell viability was subsequently measured using the Cell Counting Kit-5 (Dojindo Laboratories, Kamimasiki, Japan). The assay was performed three times.

Sphere formation assay. Cells were seeded in 96-well flat bottom ultra-low attachment culture dishes (Corning, Tewksbury, MA, USA) at 10 cells per well in ReproStem medium (ReproCELL, Yokohama, Japan) containing penicillin ($50\,U\,ml^{-1}$) and streptomycin ($50\,\mu g\,ml^{-1}$) cocktail and basic fibroblast growth factor ($5\,ng\,ml^{-1}$) without FBS. After 10 days, the size of spheroid colonies was measured under a microscope and the number of colonies with a diameter over 100 μM was counted. The assay was performed three times.

Xenograft assay. The various numbers of cells (1×10^2, 1×10^3 and 1×10^4) were diluted in equal amounts of DMEM and Matrigel (BD Biosciences) to a final volume of 200 μl then injected subcutaneously into NOD/SCID mice (Charles River Laboratories Japan, Yokohama, Japan) using a 22-gauge needle. The mice were maintained under pathogen-free conditions and sacrificed 2 months later or when tumours exceeded 20 mm at the largest diameter. Mice were handled in accordance with the procedures outlined in the Regulations on Animal Experiments at Osaka University. The institutional committee on animal research approved the study.

Quantitative real-time PCR. Quantitative real-time PCR was used to validate siRNA-mediated knockdown of CD10 and to examine mRNA levels of *OCT3/4*. Briefly, total RNA was isolated from cells using TRIzol reagent (Life Technologies) and cDNA was synthesised using the ReverTra Ace qPCR RT Master Mix (Toyobo, Osaka, Japan). Quantitative reverse transcription–PCR (qRT–PCR) was performed using a Light Cycler TaqMan Master (Roche, Basel, Switzerland). The primer sequences were as follows: CD10 5′-GGGGAGGCTTTATGTGGAAG-3′ (sense) and 3′-CTC GGATCTGTGCAATCAAA-5′ (antisense); and OCT3/4 5′-GAAA CCCACACTGCAGATCA-3′ (sense) and 3′-CGGTTACAGAACC ACACTCG-5′ (antisense). Gene expression levels were normalised to that of ACTB, 5′-AGAGCTACGAGCTGCCTGAC-3′ (sense) and 3′-CGTGGATGCCACAGGACT-5′ (antisense).

Transfection. The siRNA duplexes, si-CD10 and si-control, were obtained from Life Technologies. The si-CD10 sequences were as follows: 5′-GGCCCUUUAUGGUACAACCUCAGAA-3′ (sense) and 3′-UUCUGAGGUUGUACCAUAAAGGGCC-5′ (antisense). An initial dose-response experiment was performed according to the manufacturer's instructions to determine optimal transfection efficiency. Optimal inhibition was observed at a concentration of 10 nM siRNA at 72 h after transfection, thus further qRT–PCR analysis was done under these conditions.

Statistical analysis. The comparison of spheroid colony sizes was made using the Mann–Whitney *U-test*. The analyses of viability curves were made using two-way analysis of variance. Other statistical comparisons were made using the Student's *t*-test. Differences were considered significant when $P<0.05$. All statistical analyses were performed using JMP Pro 11 (SAS Institute, Cary, NC, USA).

RESULTS

Identification of antigens related to therapeutic resistance. To identify antigens related to therapeutic resistance, surface antigen expression levels in cells from three HNSCC cell lines, Detroit562, FaDu and BICR6 that survived treatment with cisplatin or radiation were compared with those of their untreated counterparts by means of LyoPlate (Supplementary Table 1). From this analysis, four cell surface antigens, CD10, CD15s, CD146 and

CD282, were found to be upregulated in each cell line following either treatment (Table 1).

To further test whether any of these antigens correlated with therapeutic resistance, we established the cisplatin-resistant Detroit562 cell line, which showed excellent viability even in the presence of cisplatin at a concentration as high as 100 μM (Figure 1A). The expression levels of CD10, CD15s, CD146 and CD282 were then compared between the parental and cisplatin-resistant Detroit562. Only CD10 expression levels were found to be significantly upregulated in cisplatin-resistant Detroit562 when compared with those in the parental line. Indeed, the CD10(+) subpopulation accounted for 22.5% compared with 1.4% in cisplatin-resistant Detroit562 and parental cells, respectively (Figure 1B). Of note, interdependence was not detected among the four markers (Figure 1C). These results indicate that CD10 may serve as a cell surface antigen specific to refractory HNSCC cells.

Association of CD10 with chemo and radio resistance. To further address the role of CD10 in resistance, we examined whether the CD10(+) subpopulation was chemo and/or radio resistant. To do this, CD10(+) and CD10(−) subpopulations were isolated by FACS from the FaDu and Detroit562 cell lines, and their viability after cisplatin treatment was compared. As shown in Figure 2A and B, the CD10(+) subpopulation was significantly more refractory to cisplatin than the CD10(−) subpopulation in both FaDu and Detroit562. We also examined whether CD10 affected the sensitivity of cells to fluorouracil, which is used in combination with cisplatin in the treatment of HNSCC (Kish *et al*, 1982). As shown in Figure 2C and D, the CD10(+) subpopulation was also significantly more refractory to fluorouracil in Detroit562. Next, we investigated the association between CD10 and radiation sensitivity. We found that the CD10(+) subpopulations of both FaDu and Detroit562 were significantly more radio resistant than the respective CD10(−) subpopulations (Figure 2E).

Association between CD10 and the cell cycle. Generally, cisplatin and fluorouracil affect DNA synthesis. Thus, slow-cell cycling or dormant cells (G0/G1 phase) are resistant to these chemotherapeutic agents (Barr *et al*, 2013). As for radiation, cells are most sensitive to its effects during the G2/M phase and less sensitive in G1/0 and S phases (Sinclair, 1968). We hypothesised that the chemo and radio resistance of the CD10(+) subpopulation was associated with cell cycle phase. Thus, we performed cell cycle analysis using Hoechst33342. As shown Figure 2F–G, the CD10(+) subpopulation had a greater proportion of cells in the G0/G1 phase and less in the G2/M phase than the CD10(−) subpopulation. These data indicated that the CD10(+) subpopulation of HNSCC cells was slow-cell cycling or dormant compared with the CD10(−) subpopulation.

CD10 and sphere formation ability. Given that CSCs are responsible for therapeutic resistance (Bao *et al*, 2006; Li *et al*, 2008), and are also in the dormant or slow-growing phase of the cell cycle (Holyoake *et al*, 1999), we hypothesised that CD10 might be a novel marker for CSCs in HNSCC. One of the most important characteristics of CSCs is self-renewal ability, which is assessed by sphere formation. First, we examined the distribution of CD10 in spheroid cells and control adherent cells using FACS analysis. In FaDu, 10.3% of spheroid cells and 2.1% of adherent cells were CD10(+). Similarly, 10.2% of spheroid cells and 1.7% of adherent cells were CD10(+) in Detroit562 (Figure 3A and B). Next, we compared sphere formation ability between CD10(+) and CD10(−) subpopulations. Although the morphology of spheroid colonies was similar between the two subpopulations (Figure 3C), there was a significant difference in their number. The CD10(+) subpopulation formed more spheroid colonies than the CD10(−) subpopulation in both FaDu and Detroit562 (Figure 3D–E). Moreover, colonies of the CD10(+) subpopulation were larger than those of the CD10(−) subpopulation in FaDu and Detroit562 (Figure 3F–G).

CD10 and tumourigenicity. To further address the association between CD10 and CSC properties, we examined whether CD10 modulates *in vivo* tumourigenicity. CD10(+) and CD10(−) subpopulations were sorted and individually transplanted into NOD/SCID mice. The result of the limiting dilution transplantation assay of Detroit562 cells is shown in Table 2. Briefly, when 1 000 cells were transplanted, the CD10(+) subpopulation formed tumours in six of six (100%) transplanted mice, while the CD10(−) subpopulation formed tumours in only two of six (33%) mice. Moreover, the CD10(+) subpopulation remained tumourigenic with as few as 100 cells. In contrast, there was no difference in tumourigenicity between the CD10(+) and CD10(−) subpopulations of FaDu (Supplementary Table 2), although the size of tumours formed by inoculation of 1000 cells was notably larger in the CD10(+) subpopulation than in the CD10(−) subpopulation (Supplementary Figure 1). To confirm that the histology of tumours was squamous cell carcinoma, we performed H&E staining (Figure 4A). Both FaDu and Detroit562 tumours from CD10(+) and CD10(−) subpopulations presented with squamous cell carcinoma histology and the shapes of these tumour cells were similar to those of parental cell lines.

Interrelations between CD10 and other CSC markers. It has been reported that CD44 (Prince *et al*, 2007), CD133 (Chiou *et al*, 2008) and ALDH1 (Chen *et al*, 2009) are markers of CSCs in HNSCC; thus, we examined the interdependence between CD10 and these markers. Since CD133 is not contained in the cell surface antigen array, we first assessed its expression in treated (cisplatin or radiation) and untreated FaDu cells by flow cytometry as per the conditions used in the array analysis. We found that CD133 expression was barely detectable even after the treatments

Table 1. Differentially expressed cell surface antigens in three HNSCC cell lines, Detroit562, FaDu and BICR6 following treatment with radiation or cisplatin

	Detroit562			FaDu			BICR6		
Cell surface antigen	Control (%)	RT (%)	CDDP (%)	Control (%)	RT (%)	CDDP (%)	Control (%)	RT (%)	CDDP (%)
CD10	7.5	36.5	31.8	9.5	23.1	24.3	31.2	38.1	57.6
CD15s	40.7	52.6	66.8	25.5	95.6	74.2	58.4	65.5	78.3
CD146	64.5	76.8	89.2	19.6	82.9	37.3	3.7	9.2	15.2
CD282	8.6	26.7	27.6	11.5	98.8	14.3	7.1	25.3	30.3

Abbreviations: CDDP, cisplatin; RT, radiotherapy. Control, no treatment; RT, cells were assayed 5 days after exposure to single fraction 8 Gy irradiation; CDDP, cells were assayed after exposure to 3 μM cisplatin for 7 days. Data represent the percentages of each marker as measured by flow cytometry.

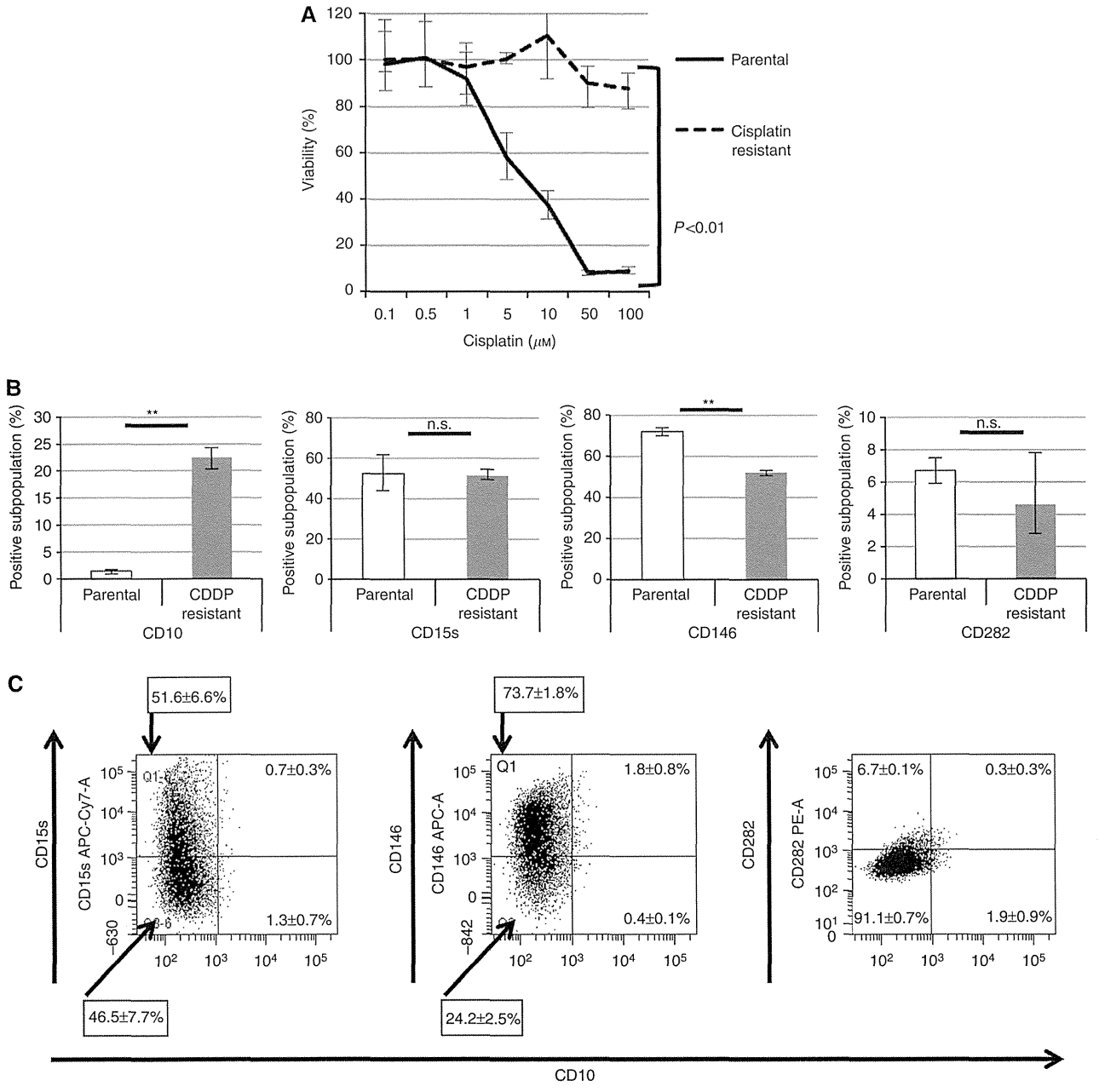

Figure 1. Expressions of candidate antigens in the cisplatin-resistant HNSCC cell line Detroit562. (**A**) Cisplatin-resistant Detroit562 were generated and validated by testing their viability against that of the parental cell line in response to cisplatin treatment, at the indicated doses. Statistical analysis was performed using two-way analysis of variance. Data represent means ± s.e.m. (**B**) Expression analyses of CD10, CD15s, CD146 and CD282 by flow cytometry in cisplatin-resistant Detroit562 and the parental cells. The percentages of positive subpopulations are indicated; $^{**}P<0.01$; n.s., not significant. (**C**) The interdependence of the four markers.

(Supplementary Table 3). Thus a relationship between CD10 and CD133 by means of FACS analysis could not be explored. As for CD44, We found that the majority of FaDu and Detroit562 cells were CD44(+). Although we found that all CD10(+) cells expressed CD44 in both Detroit562 and FaDu cell lines (Supplementary Figure 2A), significant interdependence was not detected. As for ALDH1, we found that CD10(+) cells expressed significantly more ALDH1 than CD10(−) counterparts in both cell lines (Figure 4B and Supplementary Figure 2B). The expression levels of CD10 and ALDH1 were found to be interdependent.

Stem cell-related genes in CD10-positive cells. To shed light on the molecular mechanisms underlying self-renewal ability and tumourigenicity of the CD10(+) subpopulation, we compared the expression of *OCT3/4*, a known marker of tissue stem cells (Nichols *et al*, 1998) and CSCs (Nichols *et al*, 1998), between CD10(+) and CD10(−) subpopulations. *OCT3/4* expression was significantly increased in the CD10(+) subpopulation when compared with that of the CD10(−) subpopulation in both FaDu and Detroit562 (Figure 4C). Of note, knockdown of CD10 by siRNA resulted in decreased expression of *OCT3/4* (Figure 4D and Supplementary Figure 3A–B).

DISCUSSION

In the present study, we used the novel cell surface antigens array Lyoplate to identify antigens relevant to cell survival after

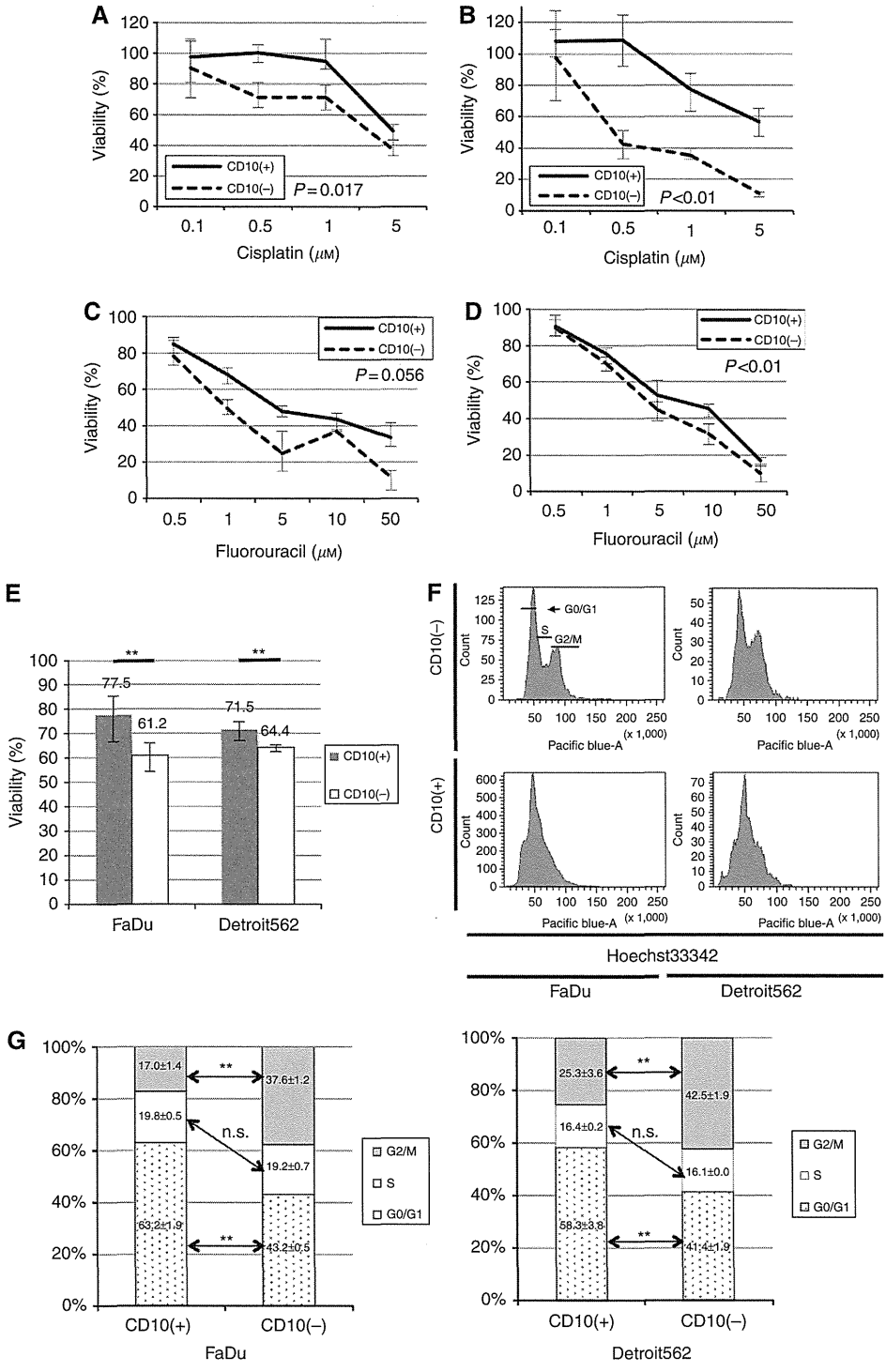

Figure 2. CD10(+)/(–) cell viability in response to treatment with cisplatin, fluorouracil, or radiation and cell cycle analysis. (**A–D**) CD10(+) and CD10(−) subpopulations were isolated by FACS and cultured with 0.1–5 μM cisplatin or 0.5–50 μM fluorouracil for 72 h. Viability in response to cisplatin in FaDu (**A**) and Detroit562 (**B**) or fluorouracil in FaDu (**C**) and Detroit562 (**D**) was then measured. Statistical analysis was performed using two-way analysis of variance. (**E**) Alternatively, cells were exposed to radiation at single fraction 8 Gy. After 72 h, cell viability was measured. Data represent means ± s.e.m.; $^{**}P<0.01$. (**F**) Cell cycle analysis of CD10-positive and -negative subpopulations was performed after staining with Hoechst33342. (**G**) The cell cycle phase distribution of CD10 (+)/(–) subpopulations. $^{**}P<0.01$; n.s., not significant.

treatment with cisplatin or radiation. This is the first report that tries to identify an antigen that exhibits both therapeutic resistance and is related to CSCs by means of the cell surface antigens array. We found that CD10, CD15s, CD146 and CD282 were highly expressed in treated cells compared with untreated cells. To validate the result of the cell surface antigens array, we next compared the expression of these antigens between a cisplatin-resistant cell line and its parental cell line. Of the candidate antigens, only expression of CD10 was upregulated in the cisplatin-resistant cell line as determined by FACS analysis. We propose two reasons for the different antigen expression profiles detected by Lyoplate and FACS analysis. First, different flow cytometers were used for the detection of signals, thus variations in sensitivity may account for the divergent findings.

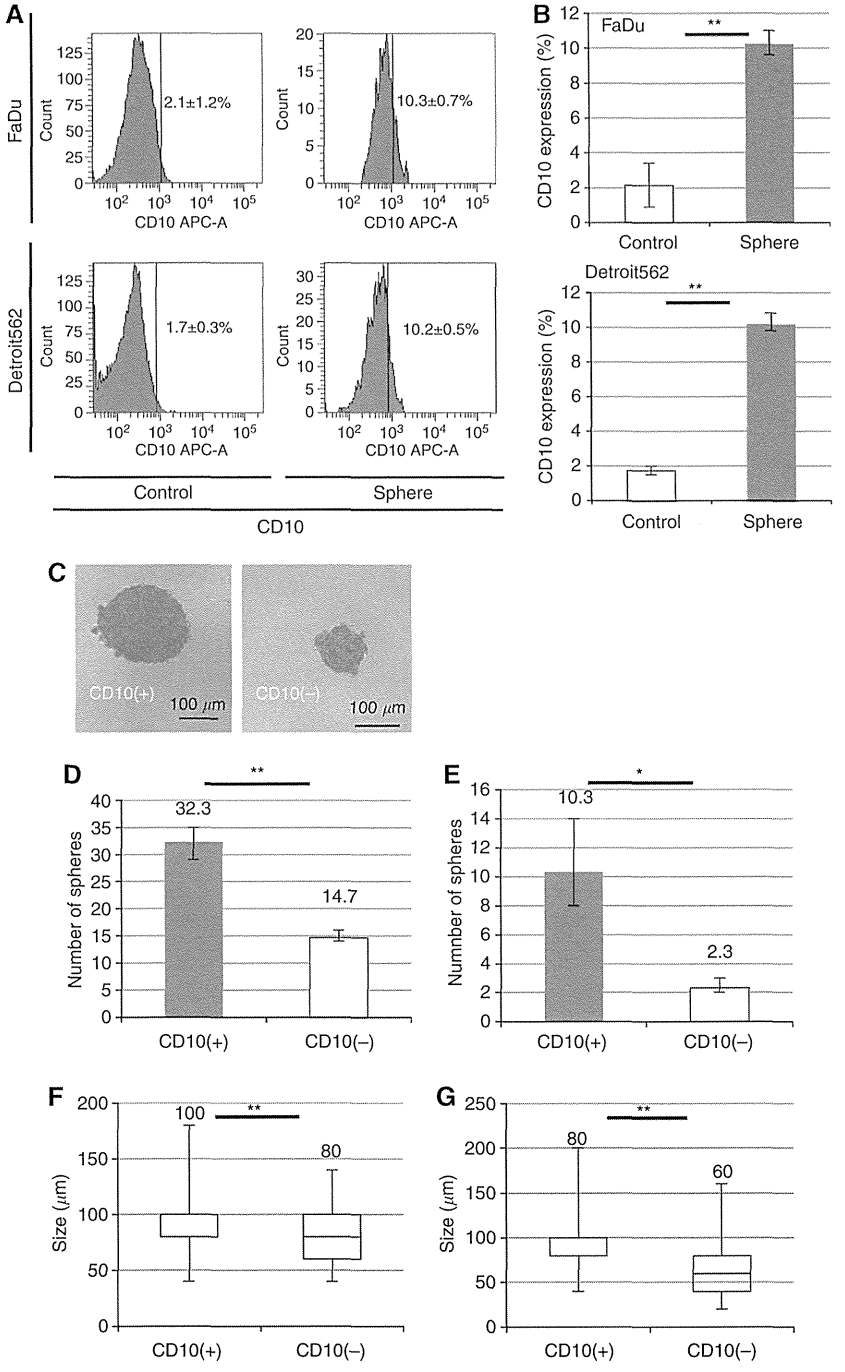

Figure 3. CD10 and sphere formation. (**A–B**) CD10 expression in sphere cells was compared with that of adherent (control) cells in FaDu and Detroit562 by flow cytometry. (**C**) CD10(+) and CD10(−) cells were sorted and the morphology of spheroid colonies in FaDu were examined. Representative images are shown. (**D–E**) The number of spheroid colonies formed in CD10(+)/(−) FaDu (**D**) and Detroit562 (**E**) were calculated. (**F–G**) The sizes of spherical colonies of CD10(+)/(−) in FaDu (**F**) and Detroit562 (**G**) were also determined. Data represent means ± s.e.m.; $^{*}P<0.05$; $^{**}P<0.01$.

Table 2. Tumourigenicity of CD10(+) and CD10(−) Detroit562 cells

No. of cells used for inoculation	No. of tumours from CD10(+) cells	No. of tumours from CD10(−) cells
10 000	4/4	4/4
1000	6/6	2/6
100	1/4	0/4

Second, it is the difference of products of antibodies such as clone number, type of fluorophores and method of staining. These may further underlie differences in technical sensitivity. However, both techniques clearly demonstrated that CD10 was upregulated in response to either cisplatin or radiation treatment, as well as in the cisplatin-resistant cell line.

CD10, also known as membrane metalloendopeptidase, neutral endopeptidase, neprilysin and common acute lymphoblastic leukaemia antigen (CALLA), is a zinc-dependent

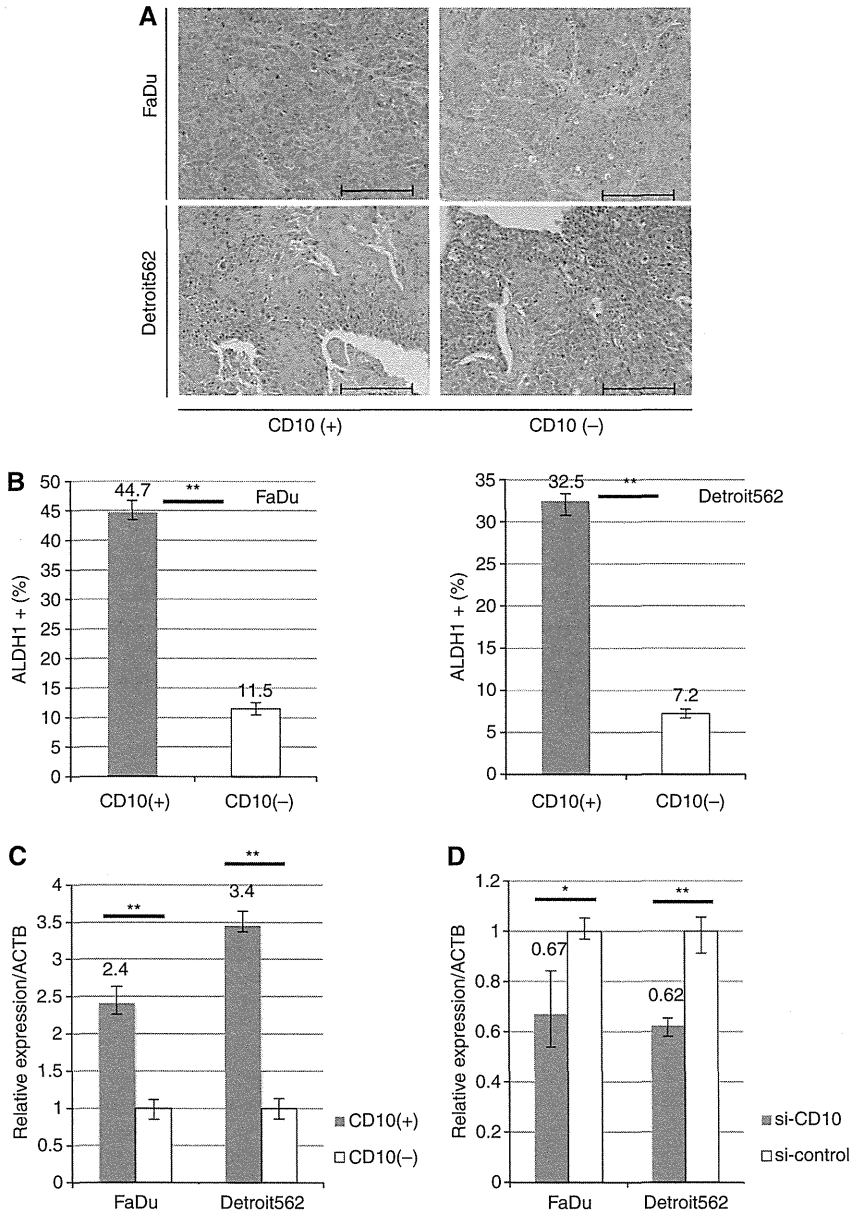

Figure 4. Histology of tumours from CD10(+)/(–) subpopulations and the relationship between CD10 and other stem cell markers. (**A**) H&E staining of FaDu and Detroit562 xenograft tumours. Scale bar, 100 μM. (**B**) Expression of ALDH1 in CD10(+)/(–) FaDu and Detroit562 cells was assessed by FACS. Data represent means ± s.e.m.; $^{**}P<0.01$. (**C**) *OCT3/4* expression in CD10(+)/(–) FaDu and Detroit562 cells was assessed by qRT–PCR. (**D**) *OCT3/4* expression in FaDu and Detroit562 following transfection with either si-CD10 or si-control was assessed by qRT–PCR. Gene expression levels are presented as a ratio of the internal control, ACTB ± s.e.m. $^{*}P<0.05$; $^{**}P<0.01$.

metalloendoprotease that cleaves signalling peptides (Roques *et al*, 1993; Turner & Tanzawa, 1997). It is expressed in a wide range of normal cells, and has been shown to be a cell surface marker of tissue stem cells in the bone marrow (Galy *et al*, 1998), adipose (Buhring *et al*, 2007), lung (Sunday *et al*, 1992) and breast (Stingl *et al*, 2005). CD10 is also expressed in a series of malignancies originating from the kidney, lung, skin, pancreas, prostate, liver, breast, stomach, cervix and bladder. Several studies have shown an association between CD10 and metastasis (Maguer-Satta *et al*, 2011). In HNSCC, an involvement of CD10 in tumour differentiation and growth has been reported (Piattelli *et al*, 2006). This report also showed that expression of CD10 was associated with distant metastases, local recurrences and histological grade in HNSCC patients. Because of this background and our experiments, we hypothesised that CD10 is a marker for refractory HNSCC. Thus, we further examined whether the CD10-positive subpopulation was chemo and/or radio resistant. We found that the CD10-positive subpopulation was more resistant to treatment with cisplatin, fluorouracil or radiation in comparison with the CD10-negative subpopulation.

Several mechanisms, such as efficient DNA repair and expression of transporter pumps, as well as changes in cell cycling are considered to explain such resistance. Among these mechanisms, we focussed on the cell cycle. We analysed cell cycle phase distributions between CD10-positive and CD10-negative subpopulations. We found that the percentage of G0/G1 phase cells was increased in CD10-positive subpopulation when compared with that of the CD10-negative subpopulation. This result indicates that the CD10-positive subpopulation of HNSCC cells was slow-cell cycling or dormant compared with CD10-negative subpopulation.

Recent studies have shown that CSCs are responsible for the therapeutic resistance of cancers (Bao *et al*, 2006; Li *et al*, 2008).